Characterizing the Diversity of Layer 2/3 Human Neocortical Neurons in Pediatric Epilepsy

J. Keenan Kushner,[1,2,3] Paige B. Hoffman,[1,3] Christine R. Brzezinski,[3] Matthew N. Svalina,[1,2,4,5] Brent R. O'Neill,[1,3] Todd C. Hankinson,[1,3] Charles C. Wilkinson,[1,3] Michael H. Handler,[1,3] Serapio M. Baca,[2,6] Molly M. Huntsman,[1,2,7] and Allyson L. Alexander[1,3]

[1]Neuroscience Graduate Program, University of Colorado | Anschutz Medical Campus, Aurora, Colorado 80045, [2]Department of Pharmaceutical Sciences, Skaggs School of Pharmacy and Pharmaceutical Sciences, University of Colorado | Anschutz Medical Campus, Aurora, Colorado 80045, [3]Department of Neurosurgery, School of Medicine, University of Colorado | Anschutz Medical Campus, Aurora, Colorado 80045, [4]Medical Scientist Training Program, University of Colorado | Anschutz Medical Campus, Aurora, Colorado 80045, [5]Department of Cell and Developmental Biology, University of Colorado | Anschutz Medical Campus, Aurora, Colorado 80045, [6]Department of Pharmacology, University of Virginia, Charlottesville, Virginia 22903, and [7]Department of Pediatrics, School of Medicine, University of Colorado | Anschutz Medical Campus, Aurora, Colorado 80045

Abstract

Childhood epilepsy is a common and devastating condition, for which many children still do not have adequate treatment. Some children with drug-resistant epilepsy require surgical excision of epileptogenic brain tissue for seizure control, affording the opportunity to study this tissue ex vivo to interrogate human epileptic neurons for potentially hyperexcitable perturbations in intrinsic electrophysiological properties. In this study, we characterized the diversity of layer L2/3 (L2/3) pyramidal neurons (PNs) in ex vivo brain slices from pediatric patients with epilepsy. We found a remarkable diversity in the firing properties of epileptic L2/3 PNs: five distinct subpopulations were identified. Additionally, we investigated whether the etiology of epilepsy influenced the intrinsic neuronal properties of L2/3 PNs when comparing tissue from patients with epilepsy due to malformations of cortical development (MCDs), other forms of epilepsy (OEs), or with deep-seated tumors. When comparing epileptic with control L2/3 PNs, we observed a decrease in voltage sag and lower maximum firing rates. Moreover, we found that MCD and OE L2/3 PNs were mostly similar indicating that epilepsy etiology may not outweigh the influences of epileptiform activity on L2/3 PN physiology. Lastly, we show that the proconvulsant drug, 4-aminopyridine (4-AP), leads to increased AP half-width, reduced firing rate accommodation, and slower AHPs. These changes imply that 4-AP induces an increase in $[K^+]_o$ and a resultant increase in AP duration, leading to the release of more excitatory neurotransmitters per action potential, thereby promoting network hyperexcitability.

Key words: DNET; focal cortical dysplasia; gliosis; layer 2/3 pyramidal neurons; intrinsic properties; tuberous sclerosis

Significance Statement

This study characterizes the diversity of L2/3 PNs within human epileptic loci ex vivo. We identify significant differences in L2/3 PN intrinsic properties between epileptic subtypes and control L2/3 PNs, and these differences promote increased synaptic summation and neurotransmission. Furthermore, we document that AHP kinetics do not dictate epileptic L2/3 PN firing rates. We also find that L2/3 PNs demonstrate commensurate properties regardless of the etiology of epilepsy. Finally, we document the effects of the convulsant drug 4-AP, on epileptic L2/3 PN intrinsic properties. This study contributes to the understanding of human neocortical epilepsy, the effects on neuron subtypes using pro-ictal drugs to generate seizures ex vivo, and the neuronal abnormalities associated with epileptogenesis.

Introduction

Childhood epilepsy is a common disorder, with a reported prevalence ranging from 0.3 to 4.4% (Camfield and Camfield, 2015; Aaberg et al., 2017). Antiseizure medications (ASMs) remain the first-line treatment for children with epilepsy, yet approximately one-third of children develop drug-resistant epilepsy and continue to have seizures (Golyala and Kwan, 2017). Malformations of cortical development (MCDs), including focal cortical dysplasia (FCD), hemimegalencephaly (HMG), and tuberous sclerosis complex (TSC), are the most common causes of surgically treated epilepsy in the pediatric population (Blumcke et al., 2017). Although surgery is curative for many patients with MCDs, not all patients are eligible for surgery and 5 year seizure freedom rates after surgery are <70% (Lamberink et al., 2020). Thus, there remains a substantial proportion of patients who continue to have seizures despite optimal medical and surgical therapy.

Over the last few decades, many studies have characterized human epileptic cortical neurons and investigated the mechanisms that underlie interictal and ictal activity (Hwa et al., 1991; D'Antuono et al., 2004; Avoli et al., 2005; Cepeda et al., 2006; Kohling and Avoli, 2006; Jacobs et al., 2008; Huberfeld et al., 2011; Talos et al., 2012; Abdijadid et al., 2015; Blauwblomme et al., 2019; Levinson et al., 2020; Rossini et al., 2021). A common neocortical layer of focus is layer 2/3 (L2/3), which controls the gain of cortical output (Quiquempoix et al., 2018). Prior pediatric MCD ex vivo studies have demonstrated that L2/3 generates ictal discharges, abnormal bursting activity, and pathogenic high-frequency oscillations (HFOs) and has shown that these epileptiform signatures are significantly regulated by NMDA receptors, GABAergic neurotransmission, and dopaminergic modulation (Wuarin et al., 1990; Cepeda et al., 1992; Mattia et al., 1995; Avoli et al., 1999; D'Antuono et al., 2004; Calcagnotto et al., 2005; Blauwblomme et al., 2019; Levinson et al., 2020). However, few of these prior studies include nonepileptic control patients or compared results between epileptic subtypes.

For many MCDs, genetic alterations in the mammalian target of rapamycin (mTOR) underlie the developmental malformation and presumably drive epileptogenesis (Jozwiak et al., 2006; Cepeda et al., 2012; O'Dell et al., 2012; Heinemann and Staley, 2014; Lipton and Sahin, 2014; Crino, 2015; Guerrini et al., 2015; D'Gama et al., 2017; Iffland and Crino, 2017; Nakagawa et al., 2017; Curatolo et al., 2018; Park et al., 2018; Wu et al., 2021). Other common pathologies leading to surgically treatable focal-onset epilepsy include perinatal stroke, often pathologically characterized by gliosis or encephalomalacia, and idiopathic forms of epilepsy, often characterized as low-grade tumors. Based on the mechanistic, developmental, and cellular differences between MCD epilepsies and other epilepsies, we hypothesized that L2/3 PNs of these subclasses differ in their intrinsic properties.

Despite the intrinsic hyperexcitability of human brain tissue resected during epilepsy surgery, ex vivo ictal activity is only induced via pharmacologic manipulations or alterations in the concentration of extracellular cations (Chang et al., 2019). One reproducible method for the generation of epileptiform activity in rodent or human tissue is wash on of 4-aminopyridine (4-AP), an A-type K^+ channel blocker (Chesnut and Swann, 1988; Avoli and Jefferys, 2016; Chang et al., 2019). Addition of 4-AP has been shown to increase action potential (AP) duration, elicit a large increase in extracellular $[K^+]$ and intracellular $[Ca^{2+}]$; generate a GABAergic, long-lasting depolarizing potential, reduce firing rate accommodation, and augment neurotransmitter release leading to interictal and ictal discharges (Lorenzon and Foehring, 1992; Kohling and Avoli, 2006; Wu et al., 2009; Abdijadid et al., 2015; Williams and Hablitz, 2015). Moreover, 4-AP allows for the examination of how voltage-gated K^+ channels (members of the Kv1, Kv3, and Kv4 families) play a role in hyperexcitability, as 4-AP has no effect on Na^+ or Ca^{2+} channels (Wulff and Zhorov, 2008). Although 4-AP can elicit ictal activity in brain slices from control and epileptic tissue, there has been little prior study of the differing effects of 4-AP on these respective tissue types. Therefore, we examined the effects of 4-AP on L2/3 PN intrinsic properties to gain a better understanding of how this potent convulsant elicits ictal activity ex vivo.

Here, we present a systematic analysis of the diversity of L2/3 PNs in human epileptic tissue. This study, to the best of our knowledge, is the first to characterize the diversity of L2/3 PNs from human epileptic foci including the differences in firing rate properties, passive membrane properties, and AP kinetics. In addition, it is the first to show differences in L2/3 PN intrinsic properties between MCD, other epilepsies, and control tissues and determines the direct effect of 4-AP on epileptic L2/3 PN intrinsic properties.

Correspondence should be addressed to J. Keenan Kushner at Keenan.Kushner@cuanschutz.edu or Allyson L. Alexander at Allyson.Alexander@childrenscolorado.org.

Materials and Methods

Acute human brain slice preparation for electrophysiology. Resected neocortical tissue was obtained from Children's Hospital Colorado. The decision to recommend epilepsy surgery is always made by a multidisciplinary team including board-certified physicians in pediatric epileptology, pediatric neurosurgery, pediatric neuroradiology, and a pediatric neuropsychologist specializing in patients with epilepsy. All patients, or their legal guardians, provided written informed consent for the study before surgery. If appropriate, the patient also provided assent. This process was performed in accordance with our institution's Institutional Review Board. For the present study, cortical tissue samples were collected from 33 patients in three experimental groups: MCD epilepsy, other epilepsy, and control. Control patients were patients with deep-seated neoplastic lesions, which required removal of normal (nonepileptogenic, non-neoplastic) superficial cortex to resect the tumor. No additional cortex was removed beyond that which was needed for resection of the deep-seated lesion. In this study, we used tissue resected from 28 epilepsy and five tumor control patients. Patients ranged from 1 to 21 years of age (mean, 9.9). Twenty were male and 13 were female. The brain samples analyzed in the present experiments were from the temporal ($n = 15$), frontal ($n = 13$), parietal ($n = 4$), or occipital ($n = 1$) neocortex. Patient information including age, sex, diagnosis, and experimental group is presented in Table 1. For all epilepsy patients, the resected neocortical tissue used for recordings was located in the epileptic focus.

Immediately following the surgical resection, resected tissue was submerged in 0–4°C carbogenated (95% O_2–5% CO_2) N-methyl-D-glucamine (NMDG) substituted artificial cerebrospinal fluid [ACSF; in mM: 92 NMDG, 2.5 KCl, 1.25 NaH_2PO_4, 30 $NaHCO_3$, 20 4-(2-hydroxyethyl)-1-pip-erazineethanesulfonic acid (HEPES), 25 D-glucose, 2 thiourea, 5 Na-ascorbate, 3 Na-pyruvate, 0.5 $CaCl_2 \cdot 4H_2O$, and 10 $MgSO_4 \cdot 7H_2O$, pH adjusted to 7.3–7.4 with concentrated hydrochloric acid (HCl), osmolality ~305 mOsm/kg]. The total duration from operating room to slicing was 15–20 min. The tissue was then placed in a carbogenated petri dish with 0–4°C carbogenated NMDG ACSF. Approximately 1 cm^3 tissue blocks were prepared with a scalpel, if the specimen was larger than that size. The arachnoid, superficial blood vessels, and cauterized tissue were carefully removed from the specimen. No effort was made to remove the pia mater due to the risk of damaging the underlying gray matter. The ~1 cm^3 tissue block was then superglued on to a vibratome stage (Leica Biosystems) and immersed in 0–4°C carbogenated NMDG ACSF. Acute coronal slices (400 μm) were prepared by slicing perpendicular to the pial surface to preserve the laminated cortical structure as well as the primary dendrites of PNs. Slices were then incubated in carbogenated NMDG ACSF at ~35°C for 12 min and were then transferred to a room temperate (~23°C) carbogenated modified HEPES ACSF (in mM: 92 NaCl, 2.5 KCl, 1.2 NaH_2PO_4, 30 $NaHCO_3$, 20 HEPES, 25 D-glucose, 2 thiourea, 5 Na-ascorbate, 3 Na-pyruvate, 2 $CaCl_2 \cdot 4H_2O$, 2 $MgSO_4 \cdot 7H_2O$, pH adjusted to 7.3–7.4 with HCl, osmolality ~305 mOsm/kg). The slices remained in the ~23°C modified HEPES ACSF for at least 30 min before being transferred to the recording chamber for electrophysiology experiments.

Electrophysiology. For whole-cell patch-clamp recordings, slices were placed in a submerged slice chamber and perfused at a rate of 2 ml/min with heated (~33°C) recording ACSF (in mM: 124 NaCl, 2.5 KCl, 1.2 NaH_2PO_4, 24 $NaHCO_3$, 5 HEPES, 12.5 D-glucose, 2 $CaCl_2 \cdot 4H_2O$, 2 $MgSO_4 \cdot 7H_2O$, pH adjusted to 7.3–7.4 with HCl, osmolality ~305 mOsm/kg). Slices were visualized using a moving stage microscope (Scientifica, SliceScope Pro 2000) equipped with 4× (0.10 NA) and a 40× water immersion objective lens (0.80 NA) objectives, differential interference contrast (DIC) optics, a SciCam Pro camera (Scientifica), and Micro-Manager 1.4 (Open Imaging). L2/3 PNs were visualized under DIC. Whole-cell patch-clamp recordings were performed with pipettes pulled to 3–6 MΩ and filled with the following internal solution (in mM: 135 potassium gluconate, 20 KCl, 10 HEPES, 0.1 EGTA, 2 Mg-ATP, 0.3 Na_2-GTP, pH adjusted to 7.3–7.4 with KOH, osmolality ~290 mOsm/kg). For most recordings, 0.4% biocytin was added to the internal solution.

After achieving whole-cell configuration, L2/3 PNs were recorded from rest in current-clamp mode ($I_{hold} = 0$ pA). Following a 0.5 s baseline period, the holding current was linearly ramped from 0 to 1,000 pA over 2 s followed by a 2.5 s recovery period. Before initiation of the series of current injections, holding current was adjusted so that the resting membrane potential of neurons was approximately −60 mV. Each cell was subjected to two series of 600 ms square current injections: −100 to +100 pA at 10 pA intervals and −250 to +1,000 pA at 50 pA intervals. The following intrinsic properties were measured in each cell using the above current injections: resting membrane potential (mV), input resistance (MΩ), membrane decay (r, ms), voltage sag (%), AP threshold, AP amplitude, AP half-width, magnitude of afterhyperpolarization (AHP, mV), AHP latency, ΔAHP, AP phase plot, AP broadening ratio, AP amplitude adaptation ratio, max firing rate (FR), FR ratio, instantaneous frequency, and frequency versus time. Extended Data Table 2-2 describes how each of the above parameters were calculated. In a subset of experiments, 100 μM of 4-aminopyridine (4-AP) was washed on to induce ictal activity. For the analysis of AHP kinetics in Figure 3, the AHPs were measured at rheobase and 2× rheobase.

Electrical recordings were acquired with a MultiClamp 700B amplifier and were sent through a Hum Bug Noise Eliminator (Quest Scientific) to then be converted to a digital signal with the Axon Digidata 1440A digitizer using pCLAMP 10.7 software (Molecular Devices). Access resistance was monitored throughout the experiments, and data were discarded if access resistance exceeded 25 MΩ. No junction potential compensation or series resistance compensation was performed. In current-clamp mode, compensation for voltage variations was achieved using a bridge balance circuit. Data were sampled at 10 kHz.

Biocytin reconstructions. After the recordings were completed, the slice was then left to rest in the recording chamber for 4–5 min to ensure transport of biocytin to distal dendrites and axon processes (Swietek et al., 2016). The slice was then fixed in 4% PFA for 24–48 h. Biocytin was visualized with streptavidin conjugated to Alexa Fluor 488 or 594 at 1:1,000 (Jackson ImmunoResearch). Biocytin-filled neurons were visualized using a Zeiss Axio Imager M2 microscope. 3D slide scanning and neuron tracing was performed using Neurolucida software (MBF Bioscience).

Statistical analyses. All data analysis was performed using MATLAB R2018a, GraphPad Prism 9.3.1, or Easy Electrophysiology v4.2.0 (http://www.easyelectrophysiology.com/). If data sets contained at least 10 data points, a D'Agostino and Pearson omnibus K2 normality test was performed to assess normality. For statistical tests between three or more groups with normally distributed data, 10 or more data points, and equal variance, an ANOVA test was performed. Equal variance was determined using the Brown–Forsythe test. If data was normally distributed but had unequal variance (Brown–Forsythe test $p < 0.05$), then a Welch's ANOVA test was performed. Following an ANOVA, a Tukey honestly significant difference (HSD) post hoc test was performed to find which group(s) differed. For statistical tests between three or more groups of non-normally distributed data, or data sets with <10 data points, a Kruskal–Wallis (KW) test was performed. Differences between groups were determined using Dunn's multiple-comparisons post hoc test and the H (degrees of freedom) statistic was checked against the critical chi-square value.

When comparing two groups with normally distributed data and standard deviations (SDs) between groups being <2×, an unpaired t test was applied. Two groups with non-normal data and/or data with SD being >2× between groups were compared using a Mann–Whitney U (MWU) test. For paired data, a paired t test was performed on normally distributed data with SD between groups being <2×, and a Wilcoxon matched-pairs signed rank test was performed on non-normal data and data where SD between groups was >2×.

All statistical tests were two-tailed. Unless otherwise stated, experimental numbers are reported as $n = x, y$, where x is the number of neurons and y is the number of patients. Statistical significance is notated in figures as the number of asterisks with the corresponding p values: *$p < 0.05$, **$p < 0.01$, ***$p < 0.001$, ****$p < 0.0001$. Data visualizations were created in MATLAB, GraphPad Prism, Adobe Illustrator, and OriginPro 2022. Data in tables and figure scatterplots are presented as mean ± SD, and figure data presented as line graphs are presented as mean ± SEM for ease of comparison. Frequency and FR ratio line graphs indicate smoothed data using the smoothing spline method in GraphPad Prism. Phase plots were created using the B-spline connect interpolation in OriginPro 2022.

Code accessibility. The MATLAB scripts used for intrinsic property analysis are from a previous publication (Guthman et al., 2020).

Results

Subjects enrolled

For this study, human neocortical tissue samples were surgically obtained from a total of 33 patients aged 1–21 years, in three histopathological groups: patients with congenital malformations of cortical development (MCD, $n = 13$), patients with other epilepsies (OE, $n = 15$), and patients with deeply located tumors and no history of seizures (control, $n = 5$). Final pathologic diagnoses were based upon examination of epileptic tissue by a board-certified pediatric neuropathologist. Classification of focal cortical dysplasias (FCDs) was based on the ILAE classification system (Blumcke et al., 2011). The experimental tissue used in this study and the tissue sent to pathology were sent from immediately adjacent areas of lesional tissue, as determined by the attending neurosurgeon. Demographic and histopathological details are presented in Table 1. We analyzed the intrinsic properties of 108 L2/3 PNs (MCD $n = 37$; other epilepsies $n = 45$; control $n = 26$). For the initial analysis of firing patterns, intrinsic properties and AHPs, presented in Figures 1–3, L2/3 PNs from both MCD and OE subgroups are combined.

Physiological diversity of L2/3 human epileptic neocortical PNs

In rodent neocortex, L2/3 PNs are a homogenous group of cells that exhibit a characteristic regular spiking phenotype. In contrast, human L2/3 PNs display diversity in their passive and active intrinsic properties, firing patterns, dendritic morphologies, and transcriptomes (DeFelipe and Farinas, 1992; Deitcher et al., 2017; Kalmbach et al., 2018; Berg et al., 2021). However, the diversity of human L2/3 PN physiological properties has not been examined in the setting of pediatric epilepsy. Therefore, we performed whole-cell patch-clamp electrophysiology on putative L2/3 PNs located within the epileptic focus from resected brain tissue of pediatric patients. We observed a considerable diversity in the firing patterns and action potential (AP) kinetics of these L2/3 PNs (Fig. 1). To confirm that we were successfully targeting L2/3 PNs in our epileptic tissue slices, 3D reconstructions of biocytin-filled neurons were performed on a subset of neurons ($n = 20$ reconstructions from 40 attempted fills). Although there was some variability in the extent of the dendritic arborization among the filled neurons, all L2/3 PNs filled with biocytin exhibited dendritic spines (data not shown) and morphologies consistent with PNs (Fig. 1; Mohan et al., 2015; Deitcher et al., 2017).

To determine if there were subtypes of epileptic putative L2/3 PNs, we first grouped them based on their action potential (AP) shape, afterhyperpolarization kinetics, and firing patterns at rheobase and 2× rheobase. Based on this initial categorization, we observed five distinct subtypes: accommodating neurons, regular spiking (RS) neurons, stuttering neurons,

Table 1. Patient information

Final pathological diagnosis	Experimental group	Region of tissue resection	Patient age at surgery (years)	Patient sex
Anaplastic Pleomorphic Xanthoastrocytoma	Control	Parietal lobe	21	M
Germinoma	Control	Parietal lobe	11	M
Embryoma	Control	Temporal lobe	9	M
Atypical meningioma	Control	Parietal lobe	8	F
Glioma	Control	Temporal lobe	1	M
FCD 1B	MCD	Temporal tip	9	F
FCD IA	MCD	Lateral temporal lobe	17	F
FCD IC	MCD	Frontal lobe, temporal tip	7	M
FCD IIA	MCD	Frontal lobe	2	F
Mild MCD	MCD	Frontal lobe	3	F
Tuberous Sclerosis	MCD	Frontal lobe	10	M
FCD IIA	MCD	Occipital lobe	19	M
FCD IIB	MCD	Frontal lobe	2	F
FCD IIID	MCD	Lateral temporal lobe	6	M
FCD IIID	MCD	Temporal lobe, frontal lobe	18	M
Tuberous Sclerosis	MCD	Temporal lobe	15	M
FCD IIA	MCD	Frontal lobe	2	F
FCD IIB	MCD	Frontal lobe	7	F
Chaslin's subpial gliosis	Other epilepsy	Lateral temporal lobe	18	M
Chaslin's subpial gliosis	Other epilepsy	Lateral temporal lobe	20	M
Encephalomalacia	Other epilepsy	Frontal lobe	18	M
Chaslin's subpial gliosis	Other epilepsy	Lateral temporal lobe	5	F
Ganglioglioma	Other epilepsy	Temporal tip	16	F
Chaslin's subpial gliosis	Other epilepsy	Frontal lobe	5	M
Chaslin's subpial gliosis	Other epilepsy	Lateral temporal lobe	10	M
Gliosis and Meningioangiomatosis	Other epilepsy	Parietal lobe	16	F
Gliosis	Other epilepsy	Frontal lobe	6	M
Gliosis	Other epilepsy	Temporal lobe	5	M
Low-grade glial neoplasm	Other epilepsy	Temporal lobe	1	F
DNET	Other epilepsy	Temporal lobe	10	F
Low-grade glioma, WHO grade I	Other epilepsy	Temporal lobe	8	M
Chaslin's subpial gliosis	Other epilepsy	Temporal lobe, frontal lobe	16	M
DNET	Other epilepsy	Frontal lobe	6	F

Demographic information, diagnosis, region of tissue resection and experimental group.

early spiking (ES) neurons, and notch neurons (Fig. 1). Accommodating neurons display significant adaptation of AP frequency and AP amplitude (Fig. 1A). RS neurons demonstrate the canonical RS AP shape and lack of accommodation in their firing pattern (Fig. 1B; Markram et al., 2015; Neske et al., 2015; Varga et al., 2015; He et al., 2016; Stedehouder et al., 2019; Berg et al., 2021; Moradi Chameh et al., 2021). Notch neurons have a fast AHP followed by an afterdepolarization (ADP; Fig. 1C; Foehring et al., 1991; Lorenzon and Foehring, 1992; Varga et al., 2015; Eyal et al., 2018). Stuttering neurons exhibit irregular firing patterns more commonly exhibited by interneurons (Fig. 1D; Druckmann et al., 2013; Stiefel et al., 2013; Komendantov et al., 2019). ES neurons exhibit a relatively hyperpolarized rheobase (Fig. 1E). Of the 82 recorded epileptic L2/3 PNs, we observed 7 accommodating neurons, 44 RS neurons, 18 notch neurons, 6 stuttering neurons, and 7 ES neurons (Fig. 2A).

After our initial classification, we analyzed the active and passive membrane properties of epileptic L2/3 PNs using a series of hyperpolarizing and depolarizing current steps (summary data and statistical analyses are presented in Table 2 and post hoc test p values in Extended Data Table 2-1). We observed no significant differences between PN subtypes in resting membrane potential (RMP, mV), input resistance (MΩ), or voltage sag (%) and found a significant difference in membrane decay time (ms) between accommodating and notch neurons (Extended Data Fig. 2-1A–D). We also observed substantial differences in AP kinetics between PN subtypes (Fig. 2B–D). More specifically, notch neurons showed the shortest AP half-width (ms) with a significant difference compared with accommodating neurons (Fig. 2E), and stuttering neurons showed the lowest spike amplitude (mV), with significant differences compared with accommodating, notch and ES neurons (Fig. 2F). Notch neurons displayed the shortest AHP latencies, with significant differences compared with RS and ES neurons, with RS neurons having a wide range of AHP latencies (Fig. 2G). We observed no subtype differences in AHP magnitude (Extended Data Fig. 2-1E). Analysis of the firing pattern within a train of APs revealed quantifiable differences between subtypes, as expected. In general, compared with other subtypes, we found that stuttering neurons were more likely to fire quickly initially and then accommodated their firing rates while ES neurons did not initially fire quickly but were the least likely to accommodate their firing rates (Fig. 2H–J). Surprisingly, we did not find differences in final instantaneous frequency (Fig. 2K, Extended Data Fig. 2-1H) or maximum firing rate (Extended Data Fig. 2-1G).
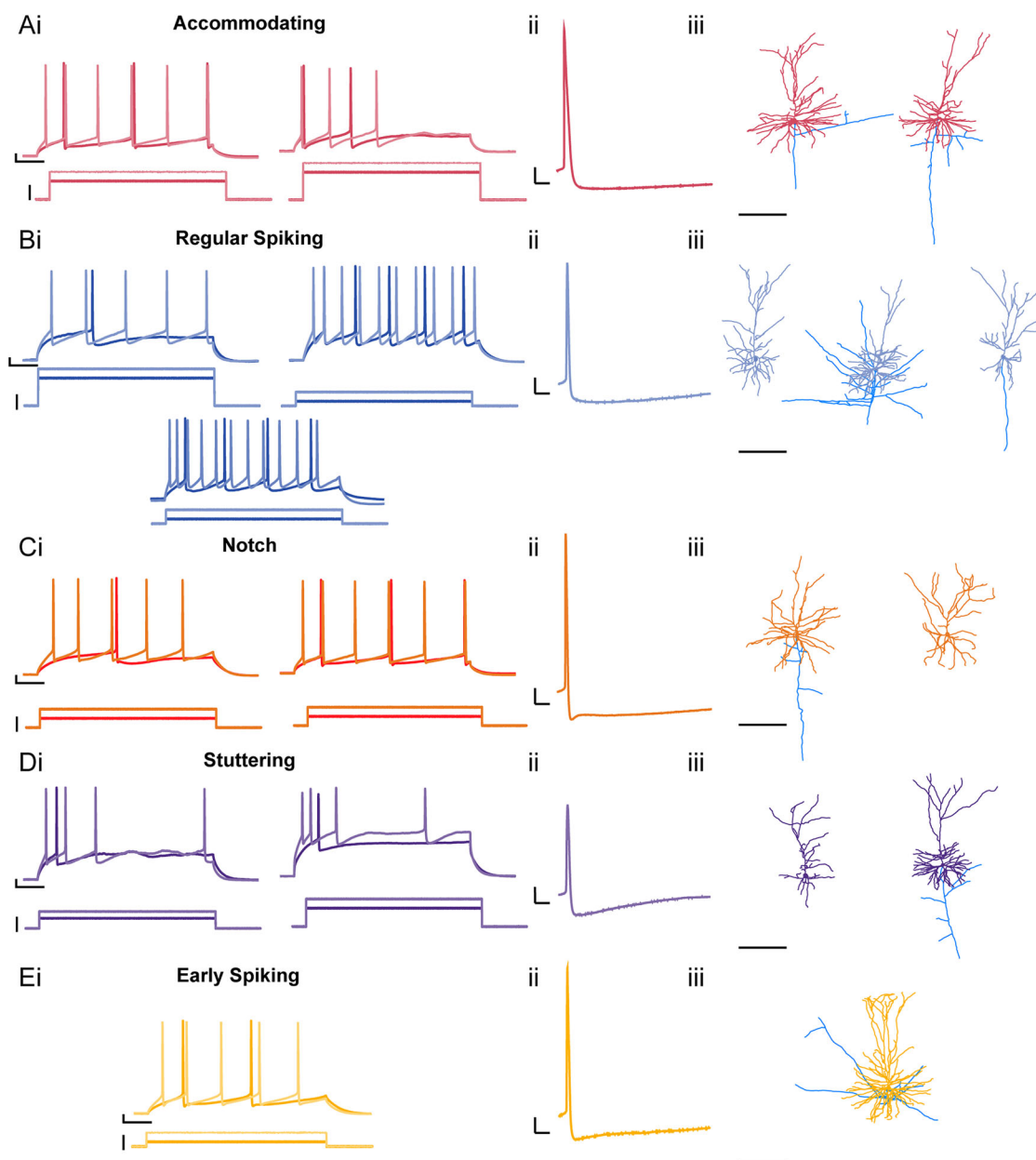
Figure 1. Putative L2/3 PNs from human epileptic foci have diverse morphology and spiking properties. ***Ai–Ei***, Depolarizing current steps at rheobase (pA; dark trace) and rheobase + 100 pA (2× rheobase, light trace) elicit action potentials (APs) of various shapes and frequencies. Each group was determined based on firing property and AHP shape. ***Aii–Eii***, Representative trace of each AP from neuron subtype (scale bars: 10 mV, 10 ms). ***Aiii–Eiii***, Corresponding 3D reconstruction of neuron morphology (x-axis scale bar: 200 μm). Each neuron's location in the representative cortical layers was determined by the respective distance of their soma from pial surface (dendrites: subtype color scheme, axon branches: blue).

Our manual classification scheme presented in Figures 1 and 2 demonstrates a high degree of physiological variability within L2/3 PNs. To determine whether these cell types could be separated mathematically, we performed an unbiased multivariable analysis using principal component analysis and *K*-means clustering using a custom-written MATLAB code. We included the six intrinsic properties that showed meaningful differences between the subtypes characterized above, including AHP latency, AP half-width, AP spike amplitude, initial ISI, FR accommodation ratio, and final ISI. We then performed a PCA using *z*-score normalized values for each property and found that three components were responsible for 76% of the total variation. Following PCA, we performed *K*-means clustering which indicated either two or five optimal clusters (Extended Data Fig. 2-2A). However, with five clusters, the majority of neurons (43/82) had silhouette values <0.5 (Extended Data Fig. 2-2B). These results indicate that PCA with *K*-means clustering did not quantifiably separate L2/3 PNs into distinct categories similar to our manually differentiated categories described above. In addition, no particular property dictated a principal component (Extended Data Fig. 2-2C). There are several possible explanations
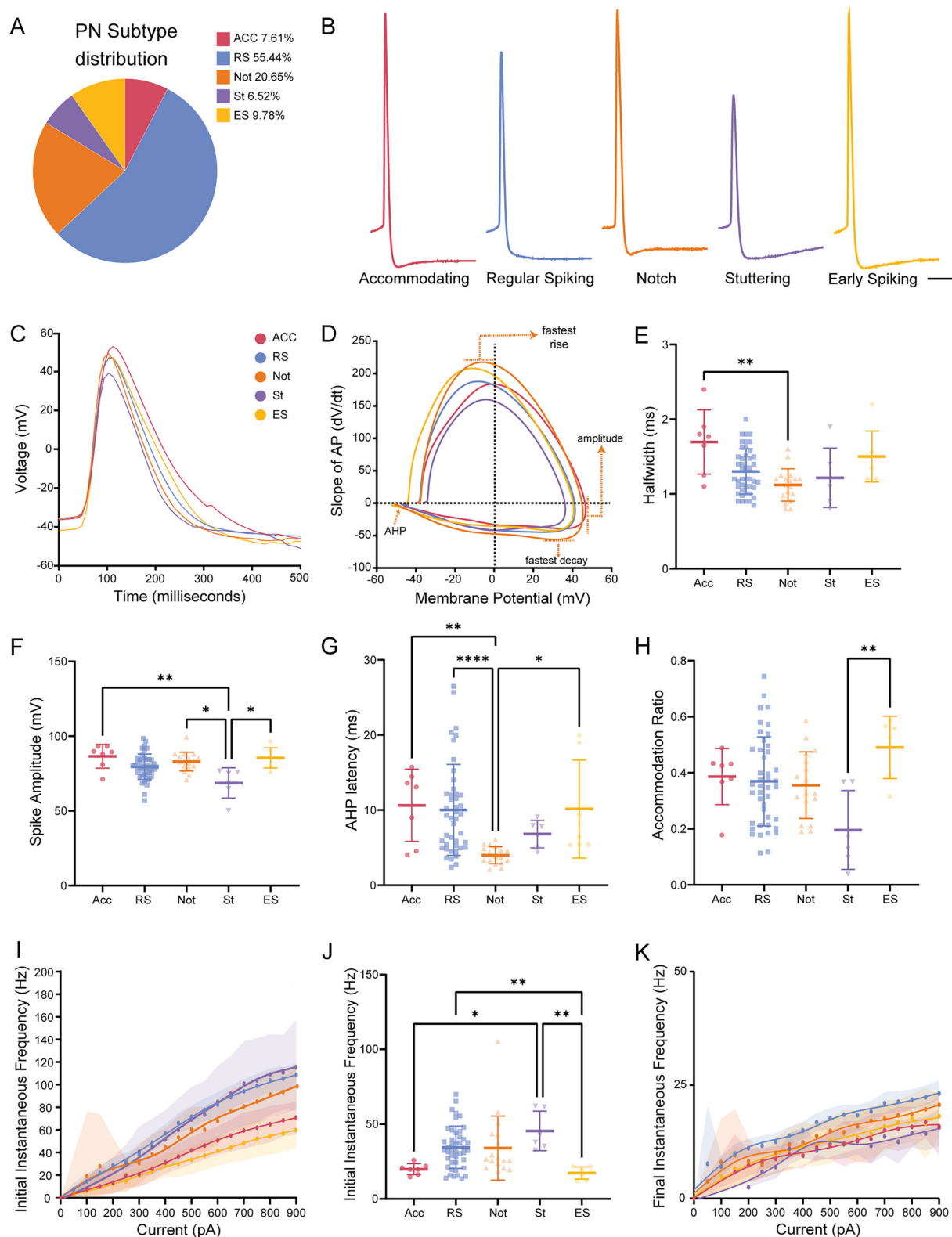
Figure 2. Putative L2/3 PN subtypes show subtle differences in AP kinetics and firing properties. **A**, Neuron subtype percentage (%) of the entire population of recorded neurons (ACC, accommodating neurons; RS, regular spiking neurons; Not, notch neurons; ST, stuttering neurons; ES, early spiking neurons). **B**, Representative traces of L2/3 PN subtype AP (scale bars: 10 mV, 10 ms). **C**, Overlay of average AP of each neuron subtype. **D**, Overlay of average phase plot (dV/dT vs voltage) indicating differences in subtype AP kinetics. **E**, Notch neurons showed the shortest AP half-width with a significant difference compared with accommodating neurons. **F**, Stutter neurons showed a significant reduction in AP spike amplitude. **G**, Notch neurons have the shortest AHP

for the different results between manual and unsupervised clustering analyses. First, it is possible that we did not measure other variables which would separate the L2/3 PNs into classes presented in Figure 1, such as transcriptomic differences. Additionally, it is possible that the observed differences in L2/3 epileptic PN intrinsic properties have minimal physiologic significance, in terms of cellular function.

Prior studies have reported that firing pattern, firing frequency, and frequency adaptation are very highly regulated by voltage-gated potassium and calcium channels that dictate AHPs (Lorenzon and Foehring, 1992; Perez-Garci et al., 2003; Phelan et al., 2005; Higgs and Spain, 2009; Rizzo et al., 2014; Mendez-Rodriguez et al., 2021). In specific relevance to the study of epilepsy, AHP duration and/or presence of an ADP has been used to classify neurons into subtypes that differ in intrinsic excitability (Phelan et al., 2005; Mendez-Rodriguez et al., 2021). Fast AHPs (fAHPs) and medium AHPs (mAHPs) can be observed following a single action potential and during repetitive firing. In some L2/3 PNs, the fAHP is followed by an ADP which drives neuronal bursting and decreases the initial interspike interval (ISI), allowing for quicker and more powerful signal transduction (Foehring et al., 1991; Higgs and Spain, 2009). However, due to its slow kinetics, the slow AHP component (sAHP, >1 s) is only observed following a period of repetitive firing, such as a burst of APs (Rizzo et al., 2014). Thus, we did not analyze the sAHP given that the differences seen in our manual analysis were seen within the train of APs generated by a depolarization.

Given that our PCA and K-means clustering did not separate neurons into distinct groups based on a set of six properties, we examined whether AHP or ADP kinetics contributed to the generation of specific L2/3 PN subtypes. For this analysis, we separated neurons into three groups (Fig. 3A): (1) neurons with a fAHP followed by an mAHP [fAHP: 16 neurons (20.25%)], (2) neurons with a fAHP-ADP-mAHP pattern [fAHP-ADP: 28 neurons (35.44%)], and (3) neurons with only an mAHP (mAHP: 35 neurons, 44.30%). We then compared the intrinsic properties of these three subsets of neurons (mean values and statistics presented in Table 3 and post hoc test p values in Extended Data Table 3-1). AP kinetics indicated no significant difference in the depolarization slope (dV/dT), but we observed a significantly higher repolarization slope in fAHP neurons compared with mAHP neurons suggesting alterations in voltage-gated potassium channel conductances (Fig. 3D,E). We also observed no significant difference in AP half-widths (Extended Data Fig. 3-1A). As expected, mAHP neurons displayed the longest AHP latencies and also displayed the largest ΔAHP magnitudes compared with fAHP and fAHP-ADP neurons (Fig. 3F,G). These results suggest that the fAHP group of neurons may have more functional BK channels while neurons without fAHPs have less BK channels and more functional SK channels, which are known to dictate mAHP amplitude (Kohling and Wolfart, 2016).

Surprisingly, we found that there were no significant differences between AHP subtypes in terms of firing patterns. More specifically, there were no significant differences in initial instantaneous frequency ($p = 0.94$, KW test), final instantaneous frequency ($p = 0.43$), mean instantaneous frequency ($p = 0.66$), or FR accommodation ratio ($p = 0.08$; Fig. 3J–M, Extended Data Fig. 3-1C–F, Table 3, Extended Data Table 3-1). We also note that accommodating, RS, and ES neurons included neurons that had all three types of AHP subsets. Notch neurons were made up of 83% fAHP-ADP PNs and 17% of fAHP PNs and stuttering neurons were all in the fAHP subtype (Fig. 3N). Together, our findings suggest that AHP and ADP kinetics do not play a significant role in determining the firing patterns of human epileptic L2/3 PNs, and therefore, the observed diversity of action potential and spiking properties are intrinsic to human epileptic L2/3 PNs and do not suggest specific subtypes of PNs with specific roles in epileptiform activity.

L2/3 PN intrinsic properties differ between histopathologic groups

In the above experiments, we grouped L2/3 PNs from patients with MCDs and other epilepsies (OEs) to demonstrate the variability of PN subtypes, given that some of the PN subtypes were relatively rare. However, we also wanted to determine if epileptic L2/3 PN intrinsic properties would differ between histopathologic groups (i.e., control, MCD, and other epilepsy). In this context, we found substantial differences in passive membrane properties and AP kinetics (mean values and statistics presented in Table 4 and post hoc test p values in Extended Data Table 4-1). Compared with control, we observed no significant difference in membrane decay but observed a significant decrease in voltage sag ratio (%) for both MCD and OE L2/3 PNs (Table 4, Extended Data Table 4-1, Fig. 4K), indicating that there may be possible alterations in I_h current. Interestingly, the decrease in epileptic L2/3 PN voltage sag compared with control L2/3 PNs correlates with extensive research demonstrating altered HCN channel expression in human and rodent epilepsies (Strauss et al., 2004; Albertson et al., 2011; Brennan et al., 2016; Lin et al., 2020; Concepcion et al., 2021). In addition, we found that MCD, but not OE, L2/3 PNs had higher input resistances compared with control (Fig. 4J). Since we observed significant variability in epileptic L2/3 PN input resistances, and previous studies have indicated that L2/3 PN morphologies change based on distance from the pial surface, we wanted to determine if the recording distance from the pial surface could potentially be contributing to this variability (Deitcher et al., 2017). Interestingly, we observed that the input resistance did not

---

latency with a significantly shorter AHP latency compared with RS and ACC neurons. **H**, FR accommodation ratio of each neuron subtype taken at 2× rheobase indicated ES neurons had a significantly lower chance of accommodating compared with stutter neurons. **I**, Initial instantaneous frequency ± SEM versus injected current (pA). **J**, Initial instantaneous frequency was taken at the rheobase + 100 pA current step and indicated significant differences between subtype initial instantaneous firing frequency. **K**, Final instantaneous frequency ± SEM versus injected current (pA). Scatterplots include mean values ± SD.
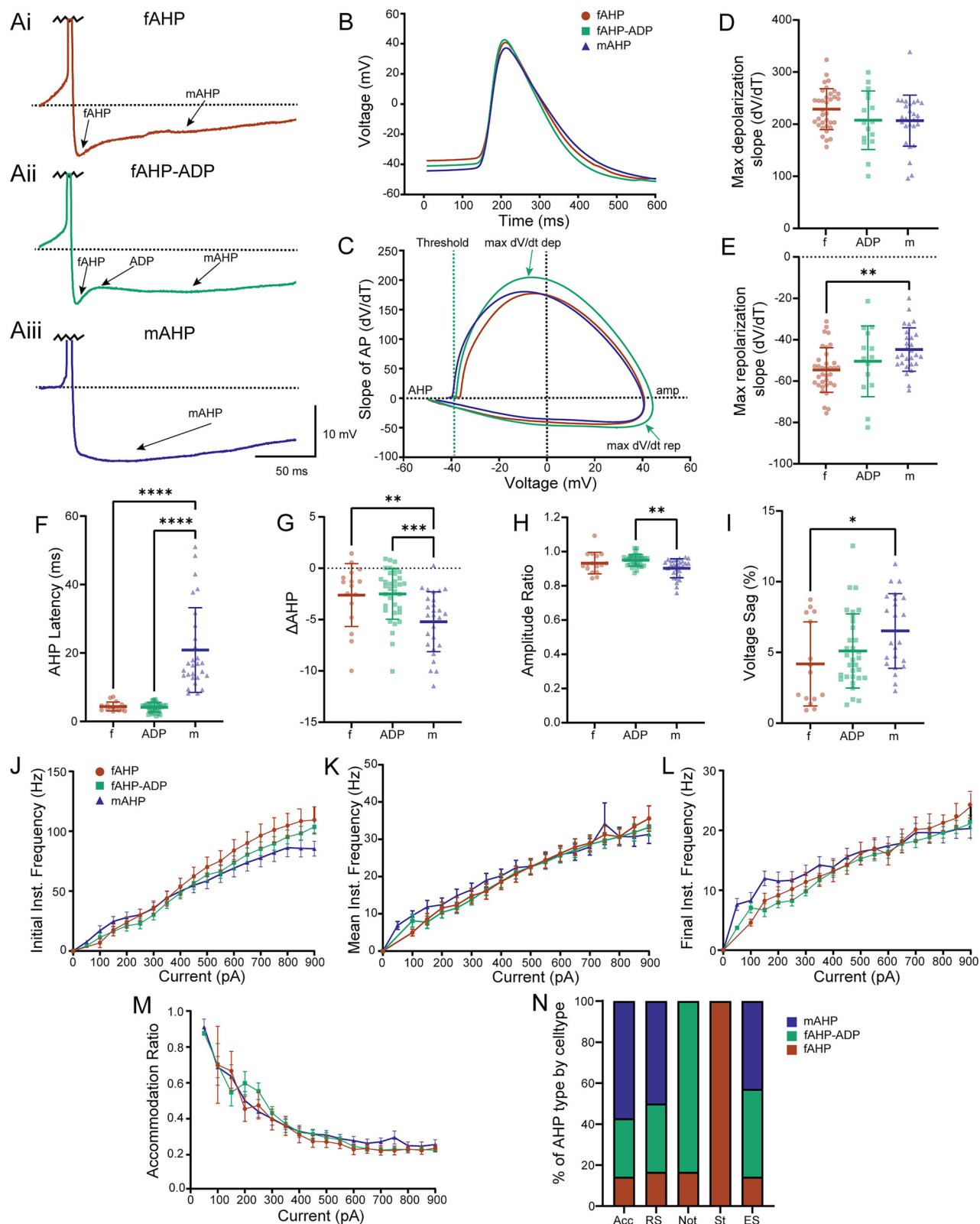
Figure 3. Epileptic L2/3 PNs with fAHP or mAHP do not differ in their firing rates or firing rate accommodation. **A**, Representative traces of L2/3 PN AP shapes showing neurons with a (**Ai**) fAHP followed by mAHP, (**Aii**) fAHP followed by ADP and mAHP, and (**Aiii**) mAHP only. **B**, Overlay of average AP of neuron split by AHP shape. **C**, Overlay of average phase plots (dV/dT vs voltage) of neuron split by AHP shape. **D**, There is no significant differences in the maximum depolarization slope of the AP (dV/dT) between subtypes. **E**, mAHP PNs have a significantly slower repolarization slope (dV/dT) when compared with fAHP PNs. **F**, AHP latency is shorter for fAHP and ADP PNs as expected compared with mAHP neurons. **G**, fAHP and ADP PNs show

Table 2. Intrinsic properties of putative L2/3 PN subtypes based on firing properties and AP shape

Intrinsic property	Accommodating ($n = 7, 4$)	Regular Spiker ($n = 44, 21$)	Notch ($n = 18, 10$)	Stutter ($n = 6, 4$)	Early Spiker ($n = 7, 6$)	KW Test (p value, H)
Resting membrane potential (mV)	-68.47 ± 7.50	-66.53 ± 7.46	-68.33 ± 2.95	-72.86 ± 5.25	-65.77 ± 5.72	$p = 0.1943$, $H_{(4)} = 6.07$
Input resistance (MΩ)	137.60 ± 68.50	136.8 ± 74.64	88.42 ± 33.15	136.10 ± 69.14	95.73 ± 44.51	$p = 0.1202$, $H_{(4)} = 7.31$
Voltage sag (%)	5.69 ± 3.27	5.27 ± 2.59	5.22 ± 2.73	4.74 ± 2.79	4.10 ± 1.14	$p = 0.8742$, $H_{(4)} = 1.22$
Membrane decay (ms)	35.34 ± 6.99	26.49 ± 7.45	24.14 ± 5.97	24.68 ± 6.95	27.03 ± 5.94	$p = 0.0340$, $H_{(4)} = 10.41$
AP threshold (mV)	-37.57 ± 3.76	-36.31 ± 5.47	-36.84 ± 3.59	-36.87 ± 10.16	-41.50 ± 5.47	$p = 0.2593$, $H_{(4)} = 5.28$
AP amplitude (mV)	86.50 ± 7.92	79.47 ± 8.54	82.98 ± 6.30	68.67 ± 10.09	85.49 ± 6.76	$p = 0.0016$, $H_{(4)} = 17.41$
AP half-width (ms)	1.69 ± 0.43	1.30 ± 0.30	1.12 ± 0.22	1.22 ± 0.40	1.5 ± 0.34	$p = 0.0062$, $H_{(4)} = 14.38$
AHP magnitude (mV)	-15.90 ± 2.71	-14.75 ± 3.67	-15.27 ± 2.55	-14.54 ± 3.14	-16.48 ± 2.61	$p = 0.7774$, $H_{(4)} = 1.77$
AHP latency (ms)	11.56 ± 8.36	14.96 ± 12.72	3.57 ± 1.12	5.05 ± 2.14	9.10 ± 5.45	$p < 0.0001$, $H_{(4)} = 25.45$
ΔAHP (mV)	-5.12 ± 3.95	-3.72 ± 3.07	-1.89 ± 1.53	-5.53 ± 2.86	-4.46 ± 2.68	$p = 0.0396$, $H_{(4)} = 10.05$
AP broadening ratio	$1.30 \pm 0 0.08$	1.27 ± 0.11	1.24 ± 0.10	1.32 ± 0.07	1.22 ± 0.07	$p = 0.1265$, $H_{(4)} = 7.18$
AP amplitude adaptation ratio	0.91 ± 0.06	0.93 ± 0.06	0.96 ± 0.04	0.91 ± 0.05	0.91 ± 0.05	$p = 0.0794$, $H_{(4)} = 8.355$
Initial instantaneous frequency (Hz)	19.88 ± 3.67	34.55 ± 14.20	34.05 ± 21.42	45.48 ± 13.20	17.27 ± 4.10	$p = 0.0002$, $H_{(4)} = 22.11$
Maximum firing rate (Hz)	24.35 ± 4.24	34.96 ± 11.76	32.94 ± 13.32	35.06 ± 8.37	23.69 ± 5.75	$p = 0.0141$, $H_{(4)} = 12.49$
Final instantaneous frequency (Hz)	8.10 ± 2.34	11.21 ± 3.37	9.59 ± 1.89	9.43 ± 7.67	8.48 ± 1.56	$p = 0.0152$, $H_{(4)} = 12.31$
Accommodation ratio	0.39 ± 0.10	0.37 ± 0.16	0.36 ± 0.12	0.20 ± 0.14	0.49 ± 0.11	$p = 0.0202$, $H_{(4)} = 11.64$

Intrinsic properties of accommodating, regular spiking, notch, stutter, and early spiking neurons.

correlate with the recorded neuron's distance from the pial surface ($r = 0.0002$, $p = 0.8522$, $n = 18$). Therefore, this variability in input resistances is most likely due to the abnormal cell types found in MCD epilepsies, such as cytomegalic/dysmorphic neurons and immature PNs (Crino, 2015; Levinson et al., 2020).

In terms of AP kinetics and firing patterns, we found no differences in AHP latency, ΔAHP, AP amplitude adaptation, or FR accommodation between control L2/3 PNs and those from epileptic foci (Table 4, Extended Data Table 4-1). However, epileptic L2/3 PNs had the propensity to generate longer AP half-widths and had significantly depolarized thresholds, slower AP depolarization slopes, and larger AHP magnitudes (Fig. 4F–I). These data suggest alterations in the expression and function of perisomatic voltage-gated sodium and potassium channels including Kv1, Kv2, Kv4, SK channels, and BK channels in epileptic L2/3 PNs. Moreover, we observed a significant decrease in epileptic L2/3 PN max FRs compared with control (Fig. 4L, right). We postulate that although epileptic foci L2/3 PNs show signs of what is canonically considered hypoexcitable, they display trends toward longer APs and reduced activation of HCN channels. Together, this may cause heightened input summation, and therefore, more excitatory neurotransmission.

Epilepsy etiology influences L2/3 PN properties

When comparing epileptic subtypes to one another, we noted few differences in intrinsic properties. Namely, the OE L2/3 PNs had lower input resistances, longer AP half-widths, larger AP amplitudes, and a lack of FR accommodation when compared with MCD L2/3 PNs (Table 4, Extended Data Table 4-1, Fig. 4G,J,M). This indicates that OE L2/3 PNs fire just as frequently (still less than control PNs) yet sustain firing with longer AP half-widths and larger AP amplitudes

←

a more positive ΔAHP. **H**, mAHP PNs have more AP amplitude adaptation compared with ADP PNs. **I**, mAHP PNs have higher overall voltage sag (%) compared with fAHP PNs. We observe no differences in **J**, initial instantaneous frequency ± SEM versus injected current (pA); **K**, mean instantaneous frequency ± SEM versus injected current (pA); **L**, final instantaneous frequency ± SEM versus injected current (pA); or **M**, FR accommodation ratio ± SEM versus injected current (pA). **N**, Percentage (%) of AHP PN based on cell type characterized in Figure 2. f, fAHP; ADP, fAHP-ADP; m mAHP. Scatterplots include mean values ± SD.

Table 3. Intrinsic properties of epileptic L2/3 PNs separated based on AHP shape and latency

Intrinsic property	fAHP neurons ($n = 16, 12$)	fAHP + ADP neurons ($n = 35, 18$)	mAHP neurons ($n = 28, 13$)	Statistical comparisons (p value)
Resting membrane potential (mV)	−70.29 ± 5.23	−68.09 ± 7.25	−65.73 ± 6.49	KW test $p = 0.0577$
Input resistance (MΩ)	135.10 ± 53.61	104.40 ± 45.38	137.90 ± 82.44	KW test $p = 0.2531$
Voltage sag (%)	4.19 ± 2.97	5.11 ± 2.61	6.51 ± 2.63	KW test $p = 0.0194$
Membrane decay (ms)	26.89 ± 6.02	26.16 ± 7.25	27.73 ± 7.29	ANOVA $p = 0.7114$
AP threshold (mV)	−35.17 ± 6.58	−37.46 ± 4.62	−37.76 ± 5.68	KW test $p = 0.6493$
AP amplitude (mV)	78.92 ± 10.74	85.02 ± 7.40	84.98 ± 8.19	KW test $p = 0.2345$
AP half-width (ms)	1.26 ± 0.35	1.26 ± 0.36	1.40 ± 0.31	KW test $p = 0.1375$
AHP magnitude (mV)	−16.42 ± 2.74	−15.25 ± 3.56	−15.14 ± 4.01	KW test $p = 0.6069$
AHP latency (ms)	4.35 ± 1.31	4.11 ± 1.36	20.84 ± 12.36	KW test $p < 0.0001$
ΔAHP (mV)	−2.61 ± 3.06	−2.49 ± 2.47	−5.21 ± 2.91	KW test $p = 0.0003$
AP broadening ratio	1.26 ± 0.09	1.26 ± 0 0.11	1.27 ± 0.10	KW test $p = 0.8880$
AP amplitude adaptation ratio	0.93 ± 0.06	0.95 ± 0.03	0.90 ± 0.05	KW test $p = 0.0026$
Initial instantaneous frequency (Hz)	32.49 ± 15.72	33.53 ± 18.93	32.30 ± 13.25	KW test $p = 0.9414$
Maximum firing rate (Hz)	37.21 ± 13.94	35.09 ± 13.10	33.67 ± 12.03	KW test $p = 0.6588$
Final instantaneous frequency (Hz)	11.43 ± 4.71	9.78 ± 2.019	11.13 ± 4.36	KW test $p = 0.4298$
Accommodation ratio	0.38 ± 0.15	0.38 ± 0.15	0.39 ± 0.13	ANOVA $p = 0.9230$
Max depolarization slope (dV/dT)	207.80 ± 56.22	228.80 ± 39.37	206.70 ± 49.12	ANOVA $p = 0.1265$
Max repolarization slope (dV/dT)	−50.44 ± 17.06	−54.64 ± 10.75	−44.74 ± 10.48	ANOVA $p = 0.0072$

Intrinsic properties of fAHP, fAHP-ADP, and mAHP epileptic L2/3 PNs.

compared with MCD L2/3 PNs. When comparing the maximum depolarization and repolarization slopes of the AP (dV/dT), we found no significant difference between epileptic subtypes. We did find that OE L2/3 PNs had slightly faster depolarizations and slower repolarizations compared with MCD L2/3 PNs. Therefore, we postulate that these intrinsic differences may be due to dysregulated transcription, post-translational modifications, or potentially somatic mutations leading to altered function of the voltage-gated channels that regulate AP kinetics (Guerrini et al., 2015; Brennan et al., 2016; Iffland and Crino, 2017; Subramanian et al., 2019).

4-AP influences L2/3 PN intrinsic properties

Acute brain slices resected from epileptic foci do not generate spontaneous seizure-like activity ex vivo. Therefore, prior studies have relied on the addition of convulsant drugs to induce epileptiform activity. 4-aminopyridine (4-AP) has been used for decades as one of these convulsant drugs and works by blocking A-type potassium currents arising from the Kv1, Kv3, and Kv4 families of potassium channels (Kohling and Avoli, 2006; Guerrini et al., 2015; Williams and Hablitz, 2015; Cepeda et al., 2018; Chang et al., 2019; Levinson et al., 2020). 4-AP has been shown to block fast AHPs, increase AP half-widths, and modulate neuron firing rates and FR adaptation (Lorenzon and Foehring, 1992; Faber and Sah, 2002). However, to our knowledge, few prior studies have investigated the direct effect of 4-AP on the intrinsic properties of L2/3 PNs from epileptic human tissue. Since 4-AP is so widely used in ex vivo epilepsy electrophysiology recordings, we believed it was critical to determine whether 4-AP affects epileptic PNs differently than nonepileptic PNs, in order to adequately interpret studies (ours and others') utilizing 4-AP to induce ictal activity in human epileptic tissue.

To this end, we performed whole-cell current-clamp recordings on L2/3 PNs and elicited hyperpolarizing and depolarizing current steps before and after 4-AP (100 µM) wash on. When comparing L2/3 PNs before and after 4-AP wash on ($n = 17, 8$), we found that 4-AP induced several alterations in epileptic L2/3 PN passive membrane properties, AP

Table 4. Intrinsic properties of L2/3 PNs split by control and epilepsy subtype

Intrinsic property	Control ($n = 26, 5$)	MCD ($n = 37, 13$)	Other epilepsies ($n = 45, 15$)	Statistical comparison (p value)
Resting membrane potential (mV)	-69.98 ± 1.19	-68.12 ± 7.13	-67.76 ± 5.20	ANOVA $p = 0.3464$
Input resistance (MΩ)	95.21 ± 36.54	137.20 ± 63.21	111.80 ± 67.72	KW test $p = 0.0068$
Voltage sag (%)	8.42 ± 4.95	5.20 ± 2.34	5.26 ± 2.88	KW test $p = 0.0137$
Membrane decay (ms)	26.23 ± 7.95	26.7 ± 7.37	26.77 ± 7.43	KW test $p = 0.9238$
AP threshold (mV)	-45.26 ± 5.61	-35.62 ± 6.09	-38.16 ± 4.75	KW test $p < 0.0001$
AP amplitude (mV)	84.07 ± 8.73	75.60 ± 8.37	84.64 ± 7.08	KW test $p < 0.0001$
AP half-width (ms)	1.33 ± 0.26	1.21 ± 0.33	1.38 ± 0.33	KW test $p = 0.0064$
AHP magnitude (mV)	-12.87 ± 3.19	-15.29 ± 3.19	-14.94 ± 3.36	ANOVA $p = 0.0102$
AHP latency (ms)	10.58 ± 5.12	8.92 ± 6.32	8.65 ± 5.56	KW test $p = 0.0843$
ΔAHP (mV)	-3.44 ± 3.10	-3.86 ± 3.28	-3.42 ± 2.73	KW test $p = 0.9027$
AP broadening ratio	1.23 ± 0.09	1.28 ± 0.10	1.25 ± 0.10	KW test $p = 0.1324$
AP amplitude adaptation ratio	0.95 ± 0.05	0.91 ± 0.06	0.94 ± 0.04	Welch's $p = 0.0421$
Maximum firing rate (Hz)	32.80 ± 10.29	26.68 ± 10.33	24.34 ± 8.10	ANOVA $p = 0.0022$
Accommodation ratio	0.46 ± 0.21	0.38 ± 0.16	0.48 ± 0.18	Welch's $p = 0.0359$
Maximum depolarization slope (dV/dT)	250.20 ± 44.25	211.80 ± 50.45	218.50 ± 48.12	ANOVA $p = 0.0062$
Maximum repolarization slope (dV/dT)	-53.85 ± 14.93	-52.61 ± 12.97	-48.26 ± 11.89	KW test $p = 0.0917$

Intrinsic properties of L2/3 PNs from control, MCD and OE ex vivo brain tissue.

properties, and firing properties (Fig. 5, Table 5). As expected, 4-AP induced an increase in AP half-width, an increase in AHP latency, a decrease in AHP magnitude, and a hyperpolarization of the AP threshold, most likely through blockade of Kv1 and Kv4 channels located at the perisomatic region and axon initial segment (Guan et al., 2006, 2007, 2013, 2015; Pathak et al., 2016; Nguyen and Anderson, 2018; Gonzalez Sabater et al., 2021; Fig. 5E–G). 4-AP had no significant effect on voltage sag (%; Table 5), AP amplitude (Fig. 5H), or max FR (Fig. 5I, right). However, 4-AP did cause a subjective increase in EPSP frequency (data not shown), induced a significant decrease in L2/3 PN input resistance, and caused significant fluctuation of FR accommodation at more depolarizing potentials (400, 500, 600, 750, 800, 850 pA steps) due to ~1-s-long sporadic hyperpolarizations (Fig. 5C,J). Lastly, we found no significant difference in the response to 4-AP between epileptic subtype L2/3 PNs [MCD ($n = 6$) and OE ($n = 11$), data not shown] suggesting that while both MCD and OE L2/3 PNs have dysfunctional Kv channel function compared with control (Fig. 4), they share similar A-Type Kv channel function (Fig. 5).

Discussion

To our knowledge, this is the first systematic study focused on characterizing intrinsic and morphological properties of human L2/3 neocortical PNs from within the epileptic focus and comparing these to control brain tissue taken from patients without any history of epilepsy. In the present study, we demonstrate clearly distinct subtypes of L2/3 PNs in human pediatric epileptic neocortex. We demonstrate that the presence of fAHPs or mAHPs do not alone dictate the excitability or firing patterns of epileptic L2/3 PNs. Additionally, we present the new finding that human epileptic L2/3 PNs exhibit reduced voltage sag, reduced max FR, and many PNs with prolonged AP half-widths compared with control PNs. These changes in intrinsic properties suggest that L2/3 PNs may allow for more synaptic input summation and increased glutamate release from a single AP. We demonstrated that there are subtle but significant differences in the intrinsic properties of L2/3 PNS from MCD and OE groups, suggesting distinct mechanisms of epileptogenesis in MCDs. Finally, we demonstrated that 4-AP leads to an increased AP half-width, a hyperpolarized AP threshold, and increased AHP magnitude in human epileptic neurons and that epileptic subtype does not dictate L2/3 PN response to 4-AP.
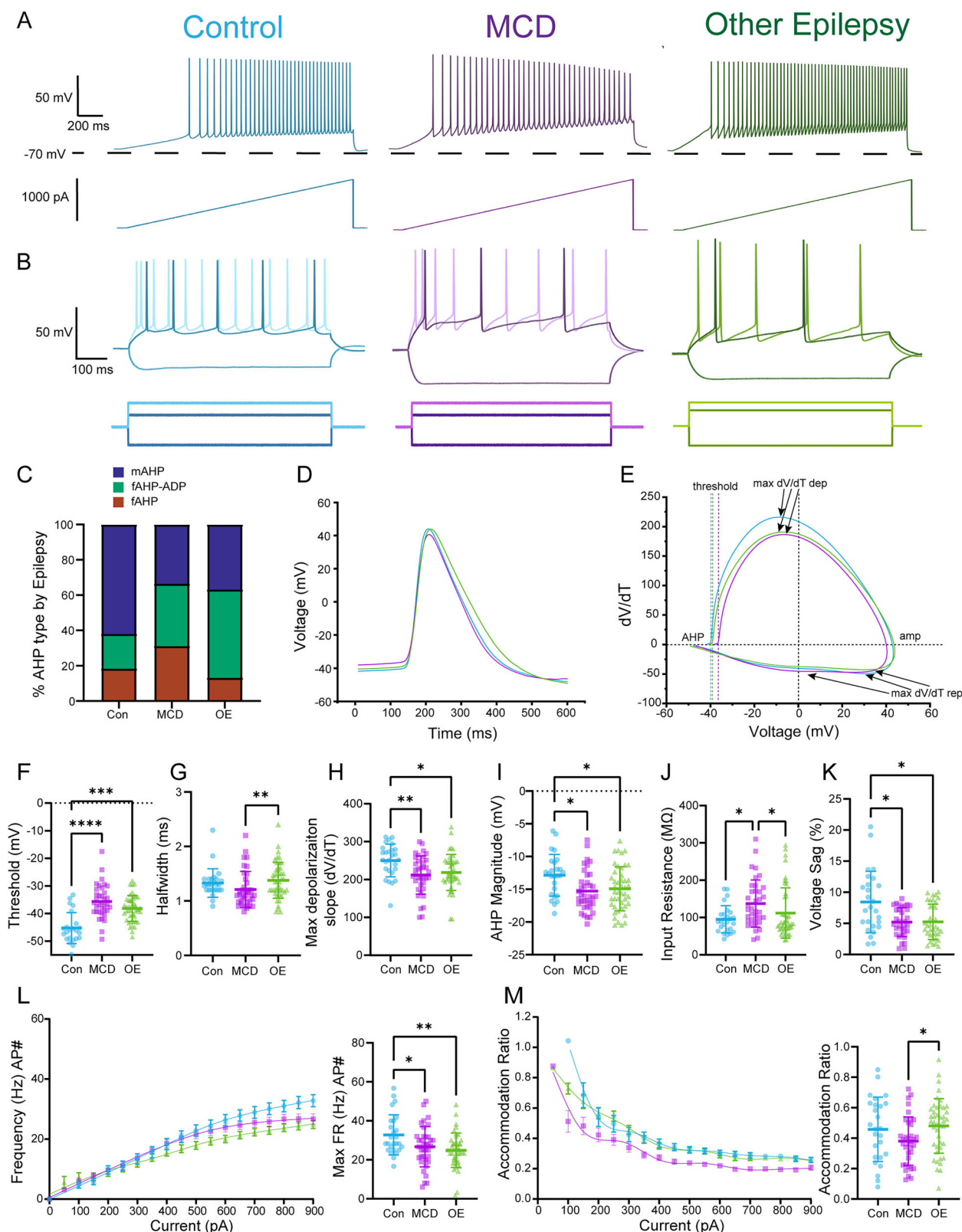
Figure 4. Epileptic L2/3 PNs show minor differences between etiology, but crucial differences compared with control neurons. **A**, Representative traces from current (pA) ramp protocol (1,000 pA, 1 s) of L2/3 PNs from control (blue), MCD epileptic (purple), and other epileptic (OE) tissue (green). **B**, Representative traces from L2/3 PNs from control and epileptic subtype showing the corresponding −250 pA hyperpolarizing step (darker negative trace), rheobase step (darker positive trace), and 2× rheobase (lighter positive trace) depolarizing current step (600 ms steps). **C**, Percentage (%) of PNs with certain AHP cell type based on control and epilepsy subtype. **D**, Overlay of average AP of control and epileptic subtype L2/3 PNs. **E**, Overlay of average phase
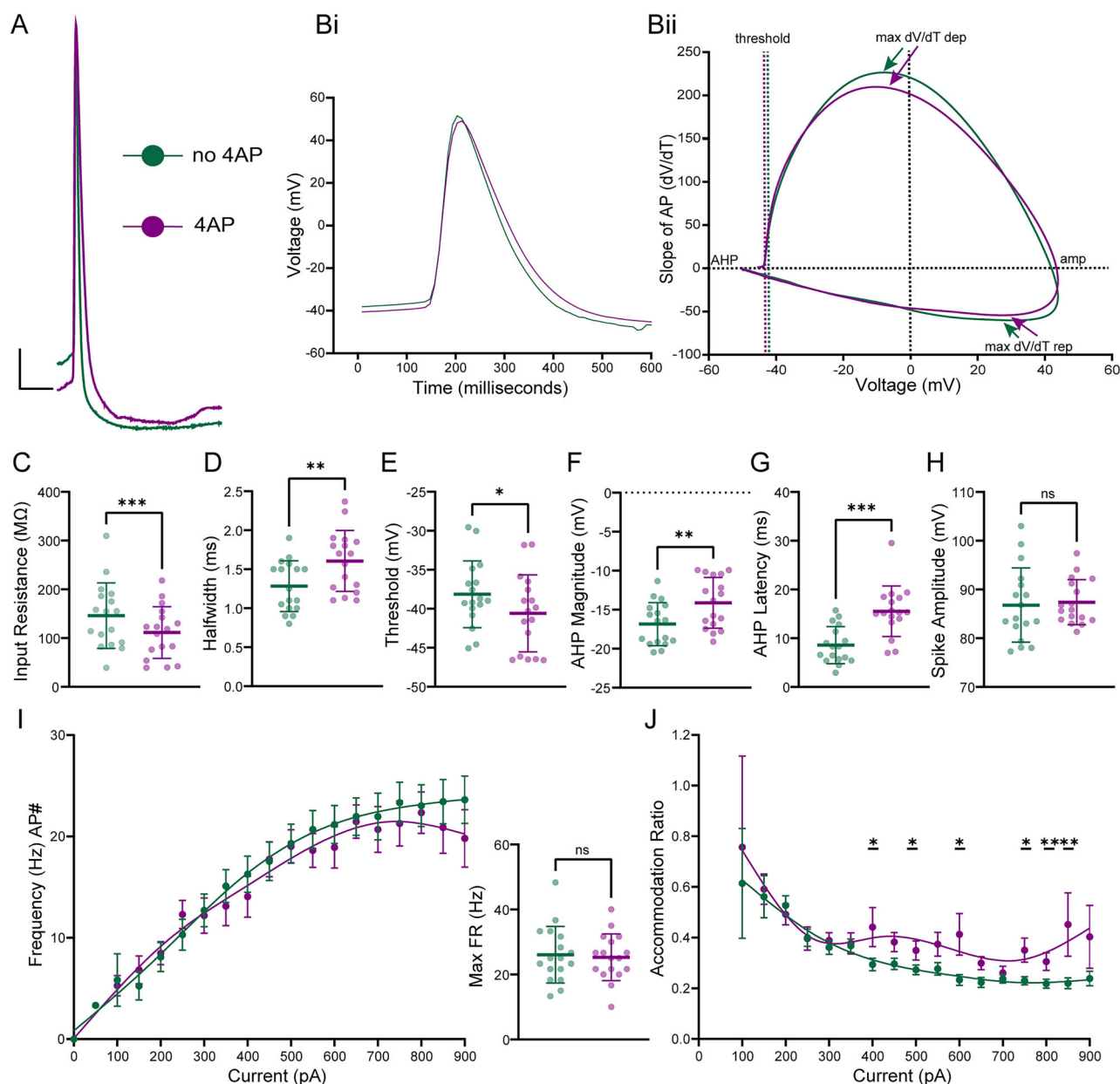
Figure 5. 4-AP increases L2/3 PN AP half-width and AHP latency and decreases AHP magnitude leading to sustained firing. **A**, Overlay of a representative AP before and after 4-AP wash on (scale bars: 10 mV, 10 ms). **Bi**, Overlay of average AP before and after 4-AP wash on. **Bii**, Overlay of phase plots. **C**, Input resistance (MΩ) decreased after 4-AP wash on. **D**, AP half-width increased after 4-AP wash on. **E**, AP threshold became hyperpolarized after 4-AP wash on. **F**, AHP magnitude was reduced after 4-AP wash on **G**, AHP latency got slower after 4-AP wash on. **H**, AP amplitude was not different after 4-AP wash on. **I**, Left, Mean FR ± SEM versus injected current (pA). **I**, Right, No significant difference was found for mean Max FR after 4-AP wash on. **J**, FR accommodation ratio ± SEM versus injected current (pA) before and after 4-AP wash on at 400, 500, 600, 750, 800, and 850 pA depolarizing current steps indicates a significant absence of accommodation after 4-AP wash on. Scatterplots include mean values ± SD.

←

plots (dV/dT vs voltage) of control and epileptic subtype L2/3 PNs. **F**, MCD L2/3 PNs have a depolarized AP threshold compared with control. **G**, OE L2/3 PNs have significantly longer AP half-widths compared with MCD with trends toward longer half-widths in both epileptic subtype PNs compared with control PNs. **H**, Depolarization slopes (dV/dT) were significantly slower in both epileptic subtypes compared with control. **I**, AHP magnitude (mV) is significantly larger in both epileptic subtypes compared with control. **J**, Epileptic L2/3 PNs show a wide variability in input resistance. MCD L2/3 PNs on average have significantly higher input resistances compared with control and OE L2/3 PNs. **K**, Voltage sag is significantly smaller in both epileptic subtypes compared with control. **L**, Left, Mean FR ± SEM versus injected current (pA). **L**, Right, We observed lower max firing rate for both epileptic subtypes compared with control. **M**, Left, FR accommodation ratio ± SEM versus injected current (pA). **M**, Right, FR accommodation ratios indicate a lack of FR accommodation by OE L2/3 PNs compared with MCD L2/3 PNs with no differences compared with control. Although, on average, control PNs accommodate their frequency the most compared with the epileptic subtype PNs. Scatterplots include mean values ± SD.

Table 5. 4-AP induces changes of epileptic L2/3 PN intrinsic properties

Intrinsic property	No 4-AP ($n = 17, 8$)	+4-AP (100 µM) ($n = 17, 8$)	Statistical comparisons (p value)
Input resistance (MΩ)	146.00 ± 67.25	111.40 ± 53.23	Paired t test $p = 0.0002$
Voltage sag (%)	6.43 ± 3.58	6.68 ± 3.48	Wilcoxon test $p = 0.3060$
Membrane decay (ms)	28.15 ± 7.90	33.38 ± 17.54	Wilcoxon test $p = 0.3303$
AP threshold (mV)	-38.14 ± 4.28	-40.59 ± 4.93	Paired t test $p = 0.0433$
AP amplitude (mV)	86.80 ± 7.62	87.40 ± 4.62	Paired t test $p = 0.7729$
AP half-width (ms)	1.28 ± 0.32	1.61 ± 0.39	Paired test $p = 0.0091$
AHP magnitude (mV)	-16.85 ± 2.76	-14.13 ± 3.26	Wilcoxon test $p = 0.0021$
AHP latency (ms)	8.59 ± 3.79	15.53 ± 5.19	Paired t test $p = 0.0002$
ΔAHP (mV)	-5.45 ± 3.22	-5.87 ± 4.50	Paired t test $p = 0.6689$
AP broadening ratio	1.26 ± 0.10	1.34 ± 0.25	Wilcoxon test $p = 0.2078$
AP amplitude adaptation ratio	0.91 ± 0.05	0.92 ± 0.07	Paired t test $p = 0.2812$
Maximum firing rate (Hz)	26.08 ± 8.70	25.29 ± 7.17	Paired t test $p = 0.3543$
Accommodation ratio (400 pA step)	0.29 ± 0.10	0.44 ± 0.29	Wilcoxon test $p = 0.0273$
Accommodation ratio (500 pA step)	0.27 ± 0.08	0.35 ± 0.16	Wilcoxon test $p = 0.0342$
Accommodation ratio (600 pA step)	0.23 ± 0.09	0.34 ± 0.13	Paired t test $p = 0.0143$
Accommodation ratio (750 pA step)	0.23 ± 0.07	0.35 ± 0.19	Wilcoxon test $p = 0.0105$
Accommodation ratio (800 pA step)	0.22 ± 0.07	0.30 ± 0.14	Wilcoxon test $p = 0.0034$
Accommodation ratio (850 pA step)	0.22 ± 0.09	0.45 ± 0.50	Wilcoxon test $p = 0.0068$

Intrinsic properties of L2/3 epileptic PNs before and after 4-AP (100 µM) wash on.

Human L2/3 PNs are intrinsically diverse

We observed that human L2/3 PNs from within the epileptic focus show a large variety of firing patterns and AP kinetics, as previously described in control L2/3 human cortical PNs (Moradi Chameh et al., 2021). Specifically, we found L2/3 PNs that exhibit regular spiking, early spiking, stuttering, and accommodating firing patterns. The last group which we termed "notch" neurons are of particular interest as they exhibit firing patterns similar to low-threshold spiking (LTS) interneurons, and yet they appear to be a subclass of PNs. Additionally, we have not encountered this cell type in mouse neocortex. In mouse cortex, LTS interneurons possess a fAHP followed by an ADP and usually express cholecystokinin (CCK), calretinin (CR), or somatostatin (SST; Beierlein et al., 2003; Tremblay et al., 2016). However, we demonstrate that morphologically, these L2/3 notch neurons are PNs. Thus, notch neurons may be a class of human L2/3 PNs not observed in mouse cortex. We postulate that the notch neuron may play a specific role in L2/3 as a network activator with the ability to vigorously respond and then adapt to a similar firing rate as RS neurons. Future studies investigating the transcriptomic profiles of the epileptic L2/3 PN subtypes, that we reported here, would help elucidate if the differences in intrinsic properties relate to gene expression profiles. Transcriptomic analysis may also provide insights into different proportions of the L2/3 PN subtypes in various subtypes of epilepsy (Berg et al., 2021).

AHP kinetics alone do not dictate firing properties of human epileptic L2/3 PNs

AHP latency and shape has previously been thought to play a critical role in dictating firing rate and firing patterns, in association with the expression of neuronal potassium channels (Avoli and Olivier, 1989; Foehring et al., 1991; Lorenzon and Foehring, 1992; Faber and Sah, 2002; Higgs and Spain, 2009; Rizzo et al., 2014; Mendez-Rodriguez et al., 2021). Similar to previous reports on human PNs, we observed epileptic L2/3 PNs with several AHP shapes and some neurons with ADPs (Foehring et al., 1991). The differences in AHP imply differences in voltage-gated potassium channels (Kv1, Kv2, and Kv4) and/or calcium-dependent potassium channels (BK and SK channels). However, contrary

to previous findings, we observed no differences in initial, maximum, or final instantaneous firing frequencies between AHP subtypes (Dodson et al., 2002; Toledo-Rodriguez et al., 2004; Guan et al., 2007, 2013; Shruti et al., 2008; Pathak et al., 2016; Rathour et al., 2016). Furthermore, we observed no differences in AHP magnitude, input resistance, or AP half-width. Our data suggest that the potassium channels that play a role in AHP shape and the corresponding firing pattern are compensatory in epileptic L2/3 PNs.

Epilepsy etiology influences L2/3 PN properties

In this study, we included specimens from patients with TSC, HME, and FCD in the MCD epilepsies group. These epileptic subtypes are characterized by disruption of the mTOR signaling pathway leading to cortical dyslamination, neuronal heterotopia, and dysmorphic neurons (Cepeda et al., 2010, 2012; Crino, 2015). Thus, we included these pathologies within a single group to determine if PI3K-AKT-mTOR pathway mutations lead to significant changes in excitatory neuron intrinsic properties (Crino, 2011; Lasarge and Danzer, 2014; Lipton and Sahin, 2014; Blumcke and Sarnat, 2016; Hanai et al., 2017; Nguyen and Anderson, 2018; Park et al., 2018). The OEs in this study included gliosis and tumor-related epilepsies. These epilepsies are not specifically related to enhanced mTOR signaling but instead, encompass a wide range of idiopathic epilepsies with most having unclear origins (Losi et al., 2012). Gliosis is a common, but nonspecific pathological finding in patients with drug-resistant epilepsies and is characterized by the presence of reactive astrocytes, which are known to release trophic factors that promote axonal sprouting and synaptic formation (O'Dell et al., 2012). In addition, astrocytes play a crucial role in neurotransmitter concentrations and the clearance of the $[K^+]_o$ via inward rectifying K^+ channels (Losi et al., 2012). Therefore, reactive astrocytes can facilitate improper synaptic transmission, shift neuronal excitability, and thereby, decrease seizure thresholds. The other, less common, OE cases were epileptic cases in which tumors caused seizures, such as glioma or dysembryoplastic neuroepithelial tumor (DNET). To our knowledge, there is no evidence that suggests that embryonic upregulation of the PI3K-AKT-mTOR pathway, which causes MCDs, is related to these cases, and in Type III FCDs, whether the congenital FCD occurs first or is a result of the neoplasia (Najm et al., 2018).

With the considerable differences in epilepsy subtypes, we determined the electrophysiological differences between their L2/3 PNs in order to further understand how epilepsy etiology can differ so significantly yet cause the same phenotype. With this in mind, we surprisingly observed only a few differences in L2/3 PN intrinsic properties between MCD and OEs. Specifically, we found OE L2/3 PNs had increased AP amplitudes, AP half-widths, lower input resistances, and less FR accommodation compared with MCD L2/3 PNs. This indicates that OE L2/3 PNs are effectively more hyperexcitable compared with MCD L2/3 PNs. We believe the differences compared with MCD L2/3 PNs may be due to maturation differences and the consequent abnormalities of morphologic and electrophysiologic properties. Nonetheless, our results suggest that epileptic L2/3 PNs across epileptic etiologies are more similar than different, and therefore, the cause of epilepsy may not outweigh the influences of seizure activity on excitatory neuron properties.

Epileptic L2/3 PNs are significantly different from tumor control L2/3 PNs

Compared with control L2/3 PNs, we observed a significant decrease in max FRs in both epileptic subtype L2/3 PNs. This was surprising considering hyperexcitable neurons are usually thought to have higher FRs. We postulate this may be a homeostatic response due to seizure activity or may result from improper neuronal development, migration, and synaptic plasticity (Andreae and Burrone, 2014; Curatolo et al., 2018; Jarero-Basulto et al., 2018; Park et al., 2018; Buchsbaum and Cappello, 2019; Medvedeva and Pierani, 2020). Furthermore, we observed that many L2/3 PNs in both epileptic subtypes possessed markedly longer AP half-widths and heightened input resistances with a considerable overlap in FRs with control PNs up to 20 Hz. When taken together, we postulate that epileptic PNs may fire less when maximally stimulated but may still release more excitatory neurotransmitters (Yang and Wang, 2006).

We also observed a reduction of voltage sag in both epileptic subtypes compared with control leading us to suspect that both MCDs and OEs lead to dysregulation of HCN channel function. In neocortical PNs, HCN channels localize primarily at the dendrites and are responsible for the I_h current, a nonspecific cation current that regulates the integration and summation of synaptic inputs (Brennan et al., 2016). I_h has previously been shown to reduce temporal summation of synaptic inputs, and therefore, reduction of I_h could lead to increased synaptic summation and contribute to network hyperexcitability (Magee, 1998; Kalmbach et al., 2018). Interestingly, dysregulated HCN channel expression and reduction in I_h current have been demonstrated in both human epilepsies and rodent epilepsy models and this dysregulation is widely considered to be proepileptogenic (Strauss et al., 2004; Brennan et al., 2016).

When comparing intrinsic properties of L2/3 PNs from MCD and control cortical tissue, we found that the MCD L2/3 PNs demonstrate a more depolarized threshold and larger AHP magnitude. One possible explanation for these findings is that an increased extracellular potassium concentration has been shown to lead to a depolarized AP threshold and increased AHP magnitude (Powell and Brown, 2021). Hyperexcitable networks often lead to increased extracellular potassium due to increased numbers of APs during ictal or interictal activity (D'Antuono et al., 2004; Avoli et al., 2005; Powell and Brown, 2021). This may also occur in OE slices as their PNs also demonstrated an increased AHP magnitude. Another explanation for these AP changes would be changes in the functionality or expression of potassium channel subunits. AP threshold is modulated by Kv1 and Kv4, whereas AHP magnitude is regulated by BK and SK channels (Lorenzon and Foehring, 1992; Pineda et al., 1992; Faber and Sah, 2002; Fernandez de Sevilla et al., 2006; Guan et al., 2007; Pathak et al., 2016).

One limitation of these comparisons is the variability in recorded cortical regions. Our control tissue included parietal and temporal lobe L2/3 PN recordings while epileptic tissue recordings were made across the cerebral cortex. Previous research has found significant differences between neocortical regions in terms of PN cytoarchitectural structure and PN intrinsic properties (Jacobs et al., 2001; DeFelipe, 2011; Mohan et al., 2015; Berg et al., 2021; Moradi Chameh et al., 2021; Benavides-Piccione et al., 2024). In this study, we utilized control tissue from patients with no history of epilepsy or use of ASMs in order to decipher the influence of ictal activity on neuronal intrinsic properties. Even at our busy neurosurgical center which performs over 800 cases per year, these samples are extremely rare. Although there are differences in the cortical origin of the control, OE, and MCD groups, we believe that the variability among cortical regions is less than the variability between phenotypes. Further research is needed to gain higher resolution of PN intrinsic properties based on cortical location and epilepsy phenotype. This limitation highlights the need for multicenter collaboration and online sharing of data in a standardized form.

4-AP influences L2/3 PN active and passive membrane properties

Prior studies on the influence of 4-AP on human neocortical neurons have shown that 4-AP abolishes the fast AHP and increases AP half-width through blockade of perisomatic Kv1 and Kv4 channels. We observed a similar effect, as 4-AP caused an increase in AP half-widths, increased AHP latencies, and decreased AHP magnitudes. To our surprise, we observed a significant decrease in input resistances after 4-AP application, which is contrary to previous reports of increased input resistance following blockade of A-type potassium channels (Rathour et al., 2016). The mechanism behind the decreased input resistances following 4-AP wash on is currently unclear but may be due to the hyperpolarizing events that occurred during current step recordings. Overall, with the increase in AP half-width, and no significant change in AP amplitude, 4-AP seemingly elicits L2/3 PNs to fire longer APs at the same efficiency most likely leading to an increase in glutamatergic neurotransmission, thereby promoting network hyperexcitability (D'Antuono et al., 2004; Avoli et al., 2005; Yang and Wang, 2006; Abdijadid et al., 2015; Dossi et al., 2024).

Potassium channels: antiseizure medications (ASMs)

Our data indicate that epileptic L2/3 PNs during pro-ictal, 4-AP administration display increased AP half-widths, hyperpolarized AP threshold, slower AHPs, and increased sustained firing at depolarized potentials. Therefore, increasing the activity of voltage-gated potassium channels at resting membrane potentials and/or stabilizing extracellular potassium could be beneficial therapeutic goals to reduce firing probability, decrease AP half-widths, and mitigate a hyperpolarized shift in AP threshold. Obviously, finding a single drug that will restore dynamic potassium channel function will be tricky. For example, there are over 80 genes for potassium channels in the human genome and previous reports indicate that both gain-of-function and loss-of-function mutations can cause seizures (Kohling and Wolfart, 2016; Zhao et al., 2024). However, as genetic testing becomes standard-of-care in patients with drug-resistant epilepsy, potassium channels should not be overlooked. Therapies aimed at correcting specific potassium channelopathies may provide significant benefit to patients.

References

Aaberg KM, Gunnes N, Bakken IJ, Lund Soraas C, Berntsen A, Magnus P, Lossius MI, Stoltenberg C, Chin R, Suren P (2017) Incidence and prevalence of childhood epilepsy: a nationwide cohort study. Pediatrics 139:e20163908.

Abdijadid S, Mathern GW, Levine MS, Cepeda C (2015) Basic mechanisms of epileptogenesis in pediatric cortical dysplasia. CNS Neurosci Ther 21:92–103.

Albertson AJ, Yang J, Hablitz JJ (2011) Decreased hyperpolarization-activated currents in layer 5 pyramidal neurons enhances excitability in focal cortical dysplasia. J Neurophysiol 106:2189–2200.

Andreae LC, Burrone J (2014) The role of neuronal activity and transmitter release on synapse formation. Curr Opin Neurobiol 27:47–52.

Avoli M, Bernasconi A, Mattia D, Olivier A, Hwa GG (1999) Epileptiform discharges in the human dysplastic neocortex: in vitro physiology and pharmacology. Ann Neurol 46:816–826.

Avoli M, Jefferys JG (2016) Models of drug-induced epileptiform synchronization in vitro. J Neurosci Methods 260:26–32.

Avoli M, Louvel J, Pumain R, Kohling R (2005) Cellular and molecular mechanisms of epilepsy in the human brain. Prog Neurobiol 77:166–200.

Avoli M, Olivier A (1989) Electrophysiological properties and synaptic responses in the deep layers of the human epileptogenic neocortex in vitro. J Neurophysiol 61:589–606.

Beierlein M, Gibson JR, Connors BW (2003) Two dynamically distinct inhibitory networks in layer 4 of the neocortex. J Neurophysiol 90:2987–5987.

Benavides-Piccione R, Blazquez-Llorca L, Kastanauskaite A, Fernaud-Espinosa I, Tapia-Gonzalez S, DeFelipe J (2024) Key morphological features of human pyramidal neurons. Cereb Cortex 34:bhae180.

Berg J, et al. (2021) Human neocortical expansion involves glutamatergic neuron diversification. Nature 598:151–158.

Blauwblomme T, Dossi E, Pellegrino C, Goubert E, Iglesias BG, Sainte-Rose C, Rouach N, Nabbout R, Huberfeld G (2019) Gamma-aminobutyric acidergic transmission underlies interictal epileptogenicity in pediatric focal cortical dysplasia. Ann Neurol 85:204–217.

Blumcke I, et al. (2011) The clinicopathologic spectrum of focal cortical dysplasias: a consensus classification proposed by an ad hoc task force of the ILAE Diagnostic Methods Commission. Epilepsia 52:158–174.

Blumcke I, et al. (2017) Histopathological findings in brain tissue obtained during epilepsy surgery. N Engl J Med 377:1648–1656.

Blumcke I, Sarnat HB (2016) Somatic mutations rather than viral infection classify focal cortical dysplasia type II as mTORopathy. Curr Opin Neurol 29:388–395.

Brennan GP, Baram TZ, Poolos NP (2016) Hyperpolarization-activated cyclic nucleotide-gated (HCN) channels in epilepsy. Cold Spring Harb Perspect Med 6:a022384.

Buchsbaum IY, Cappello S (2019) Neuronal migration in the CNS during development and disease: insights from in vivo and in vitro models. Development 146:dev163766.

Calcagnotto ME, Paredes MF, Tihan T, Barbaro NM, Baraban SC (2005) Dysfunction of synaptic inhibition in epilepsy associated with focal cortical dysplasia. J Neurosci 25:9649–9657.

Camfield P, Camfield C (2015) Incidence, prevalence and aetiology of seizures and epilepsy in children. Epileptic Disord 17:117–123.

Cepeda C, et al. (2012) Enhanced GABAergic network and receptor function in pediatric cortical dysplasia type IIB compared with tuberous sclerosis complex. Neurobiol Dis 45:310–321.

Cepeda C, Andre VM, Levine MS, Salamon N, Miyata H, Vinters HV, Mathern GW (2006) Epileptogenesis in pediatric cortical dysplasia: the dysmature cerebral developmental hypothesis. Epilepsy Behav 9:219–235.

Cepeda C, Andre VM, Yamazaki I, Hauptman JS, Chen JY, Vinters HV, Mathern GW, Levine MS (2010) Comparative study of cellular and synaptic abnormalities in brain tissue samples from pediatric tuberous sclerosis complex and cortical dysplasia type II. Epilepsia 51:160–165.

Cepeda C, Levinson S, Yazon VW, Barry J, Mathern GW, Fallah A, Vinters HV, Levine MS, Wu JY (2018) Cellular antiseizure mechanisms of everolimus in pediatric tuberous sclerosis complex, cortical dysplasia, and non-mTOR-mediated etiologies. Epilepsia Open 3:180–190.

Cepeda C, Radisavljevic Z, Peacock W, Levine MS, Buchwald NA (1992) Differential modulation by dopamine of responses evoked by excitatory amino acids in human cortex. Synapse 11:330–341.

Chang M, Dufour S, Carlen PL, Valiante TA (2019) Generation and on-demand initiation of acute ictal activity in rodent and human tissue. J Vis Exp 143:e57952.

Chesnut TJ, Swann JW (1988) Epileptiform activity induced by 4-aminopyridine in immature hippocampus. Epilepsy Res 2:187–195.

Concepcion FA, Khan MN, Ju Wang JD, Wei AD, Ojemann JG, Ko AL, Shi Y, Eng JK, Ramirez JM, Poolos NP (2021) HCN channel phosphorylation sites mapped by mass spectrometry in human epilepsy patients and in an animal model of temporal lobe epilepsy. Neuroscience 460:13–30.

Crino PB (2011) mTOR: a pathogenic signaling pathway in developmental brain malformations. Trends Mol Med 17:734–742.

Crino PB (2015) Focal cortical dysplasia. Semin Neurol 35:201–208.

Curatolo P, Moavero R, van Scheppingen J, Aronica E (2018) mTOR dysregulation and tuberous sclerosis-related epilepsy. Expert Rev Neurother 18:185–201.

D'Antuono M, Louvel J, Kohling R, Mattia D, Bernasconi A, Olivier A, Turak B, Devaux A, Pumain R, Avoli M (2004) GABAA receptor-dependent synchronization leads to ictogenesis in the human dysplastic cortex. Brain 127:1626–1640.

DeFelipe J (2011) The evolution of the brain, the human nature of cortical circuits, and intellectual creativity. Front Neuroanat 5:29.

DeFelipe J, Farinas I (1992) The pyramidal neuron of the cerebral cortex: morphological and chemical characteristics of the synaptic inputs. Prog Neurobiol 39:563–607.

Deitcher Y, Eyal G, Kanari L, Verhoog MB, Atenekeng Kahou GA, Mansvelder HD, de Kock CPJ, Segev I (2017) Comprehensive morpho-electrotonic analysis shows 2 distinct classes of L2 and L3 pyramidal neurons in human temporal cortex. Cereb Cortex 27:5398–5414.

D'Gama AM, et al. (2017) Somatic mutations activating the mTOR pathway in dorsal telencephalic progenitors cause a continuum of cortical dysplasias. Cell Rep 21:3754–3766.

Dodson PD, Barker MC, Forsythe ID (2002) Two heteromeric Kv1 potassium channels differentially regulate action potential firing. J Neurosci 22:6953–6961.

Dossi E, Zonca L, Pivonkova H, Milior G, Moulard J, Vargova L, Chever O, Holcman D, Rouach N (2024) Astroglial gap junctions strengthen hippocampal network activity by sustaining afterhyperpolarization via KCNQ channels. Cell Rep 43:114158.

Druckmann S, Hill S, Schurmann F, Markram H, Segev I (2013) A hierarchical structure of cortical interneuron electrical diversity revealed by automated statistical analysis. Cereb Cortex 23:2994–3006.

Eyal G, Verhoog MB, Testa-Silva G, Deitcher Y, Benavides-Piccione R, DeFelipe J, de Kock CPJ, Mansvelder HD, Segev I (2018) Human cortical pyramidal neurons: from spines to spikes via models. Front Cell Neurosci 12:181.

Faber ES, Sah P (2002) Physiological role of calcium-activated potassium currents in the rat lateral amygdala. J Neurosci 22:1618–1628.

Fernandez de Sevilla D, Garduno J, Galvan E, Buno W (2006) Calcium-activated afterhyperpolarizations regulate synchronization and timing of epileptiform bursts in hippocampal CA3 pyramidal neurons. J Neurophysiol 96:3028–3041.

Foehring RC, Lorenzon NM, Herron P, Wilson CJ (1991) Correlation of physiologically and morphologically identified neuronal types in human association cortex in vitro. J Neurophysiol 66:1825–1837.

Golyala A, Kwan P (2017) Drug development for refractory epilepsy: the past 25 years and beyond. Seizure 44:147–156.

Gonzalez Sabater V, Rigby M, Burrone J (2021) Voltage-gated potassium channels ensure action potential shape fidelity in distal axons. J Neurosci 41:5372–5385.

Guan D, Armstrong WE, Foehring RC (2013) Kv2 channels regulate firing rate in pyramidal neurons from rat sensorimotor cortex. J Physiol 591:4807–4825.

Guan D, Armstrong WE, Foehring RC (2015) Electrophysiological properties of genetically identified subtypes of layer 5 neocortical pyramidal neurons: Ca(2)(+) dependence and differential modulation by norepinephrine. J Neurophysiol 113:2014–2032.

Guan D, Lee JC, Higgs MH, Spain WJ, Foehring RC (2007) Functional roles of Kv1 channels in neocortical pyramidal neurons. J Neurophysiol 97:1931–1940.

Guan D, Lee JC, Tkatch T, Surmeier DJ, Armstrong WE, Foehring RC (2006) Expression and biophysical properties of Kv1 channels in supragranular neocortical pyramidal neurones. J Physiol 571:371–389.

Guerrini R, et al. (2015) Diagnostic methods and treatment options for focal cortical dysplasia. Epilepsia 56:1669–1686.

Guthman EM, Garcia JD, Ma M, Chu P, Baca SM, Smith KR, Restrepo D, Huntsman MM (2020) Cell-type-specific control of basolateral amygdala neuronal circuits via entorhinal cortex-driven feedforward inhibition. Elife 9:e50601.

Hanai S, et al. (2017) Pathologic active mTOR mutation in brain malformation with intractable epilepsy leads to cell-autonomous migration delay. Am J Pathol 187:1177–1185.

He M, et al. (2016) Strategies and tools for combinatorial targeting of GABAergic neurons in mouse cerebral cortex. Neuron 91:1228–1243.

Heinemann U, Staley KJ (2014) What is the clinical relevance of in vitro epileptiform activity? In: *Issues in clinical epileptology: a view from the bench*, Ed 1, (Scharfman HE, Buckmaster PS, eds), pp 25–41. Dordrecht: Springer.

Higgs MH, Spain WJ (2009) Conditional bursting enhances resonant firing in neocortical layer 2-3 pyramidal neurons. J Neurosci 29:1285–1299.

Huberfeld G, Menendez de la Prida L, Pallud J, Cohen I, Le Van QuyenM, Adam C, Clemenceau S, Baulac M, Miles R (2011) Glutamatergic pre-ictal discharges emerge at the transition to seizure in human epilepsy. Nat Neurosci 14:627–634.

Hwa GG, Avoli M, Oliver A, Villemure JG (1991) Bicuculline-induced epileptogenesis in the human neocortex maintained in vitro. Exp Brain Res 83:329–339.

Iffland PH 2nd, Crino PB (2017) Focal cortical dysplasia: gene mutations, cell signaling, and therapeutic implications. Annu Rev Pathol 12:547–571.

Jacobs J, LeVan P, Chander R, Hall J, Dubeau F, Gotman J (2008) Interictal high-frequency oscillations (80-500Hz) are an indicator of seizure onset areas independent of spikes in the human epileptic brain. Epilepsia 49:1893–1907.

Jacobs B, Schall M, Prather M, Kapler E, Driscoll L, Baca S, Jacobs J, Ford K, Wainwright M, Treml M (2001) Regional dendritic and spine variation in human cerebral cortex: a quantitative Golgi study. Cereb Cortex 11:558–571.

Jarero-Basulto JJ, Gasca-Martinez Y, Rivera-Cervantes MC, Urena-Guerrero ME, Feria-Velasco AI, Beas-Zarate C (2018) Interactions between epilepsy and plasticity. Pharmaceuticals 11:17.

Jozwiak J, Kotulska K, Jozwiak S (2006) Similarity of balloon cells in focal cortical dysplasia to giant cells in tuberous sclerosis. Epilepsia 47:805.

Kalmbach BE, et al. (2018) h-Channels contribute to divergent intrinsic membrane properties of supragranular pyramidal neurons in human versus mouse cerebral cortex. Neuron 100:1194–1208.e5.

Kohling R, Avoli M (2006) Methodological approaches to exploring epileptic disorders in the human brain in vitro. J Neurosci Methods 155:1–19.

Kohling R, Wolfart J (2016) Potassium channels in epilepsy. Cold Spring Harb Perspect Med 6:a022871.

Komendantov AO, Venkadesh S, Rees CL, Wheeler DW, Hamilton DJ, Ascoli GA (2019) Quantitative firing pattern phenotyping of hippocampal neuron types. Sci Rep 9:17915.

Lamberink HJ, Otte WM, Blumcke I, Braun KPJ, European Epilepsy Brain Bank Writing Group, Study Group, European Reference Network EpiCARE (2020) Seizure outcome and use of antiepileptic drugs after epilepsy surgery according to histopathological diagnosis: a retrospective multicentre cohort study. Lancet Neurol 19:748–757.

Lasarge CL, Danzer SC (2014) Mechanisms regulating neuronal excitability and seizure development following mTOR pathway hyperactivation. Front Mol Neurosci 7:18.

Levinson S, Tran CH, Barry J, Viker B, Levine MS, Vinters HV, Mathern GW, Cepeda C (2020) Paroxysmal discharges in tissue slices from pediatric epilepsy surgery patients: critical role of GABA(B) receptors in the generation of ictal activity. Front Cell Neurosci 14:54.

Lin W, et al. (2020) Downregulation of hyperpolarization-activated cyclic nucleotide-gated channels (HCN) in the hippocampus of patients with medial temporal lobe epilepsy and hippocampal sclerosis (MTLE-HS). Hippocampus 30:1112–1126.

Lipton JO, Sahin M (2014) The neurology of mTOR. Neuron 84:275–291.

Lorenzon NM, Foehring RC (1992) Relationship between repetitive firing and afterhyperpolarizations in human neocortical neurons. J Neurophysiol 67:350–363.

Losi G, Cammarota M, Carmignoto G (2012) The role of astroglia in the epileptic brain. Front Pharmacol 3:132.

Magee JC (1998) Dendritic hyperpolarization-activated currents modify the integrative properties of hippocampal CA1 pyramidal neurons. J Neurosci 18:7613–7624.

Markram H, et al. (2015) Reconstruction and simulation of neocortical microcircuitry. Cell 163:456–492.

Mattia D, Olivier A, Avoli M (1995) Seizure-like discharges recorded in human dysplastic neocortex maintained in vitro. Neurology 45:1391–1395.

Medvedeva VP, Pierani A (2020) How do electric fields coordinate neuronal migration and maturation in the developing cortex? Front Cell Dev Biol 8:580657.

Mendez-Rodriguez BS, Arias-Garcia MA, Tapia D, Laville A, Bargas J, Galarraga E (2021) Firing differences between adult intralaminar thalamo-striatal neurons. Neuroscience 458:153–165.

Mohan H, et al. (2015) Dendritic and axonal architecture of individual pyramidal neurons across layers of adult human neocortex. Cereb Cortex 25:4839–4853.

Moradi Chameh H, Rich S, Wang L, Chen FD, Zhang L, Carlen PL, Tripathy SJ, Valiante TA (2021) Diversity amongst human cortical pyramidal neurons revealed via their sag currents and frequency preferences. Nat Commun 12:2497.

Najm IM, Sarnat HB, Blumcke I (2018) Review: the international consensus classification of focal cortical dysplasia - a critical update 2018. Neuropathol Appl Neurobiol 44:18–31.

Nakagawa JM, Donkels C, Fauser S, Schulze-Bonhage A, Prinz M, Zentner J, Haas CA (2017) Characterization of focal cortical dysplasia with balloon cells by layer-specific markers: evidence for differential vulnerability of interneurons. Epilepsia 58:635–645.

Neske GT, Patrick SL, Connors BW (2015) Contributions of diverse excitatory and inhibitory neurons to recurrent network activity in cerebral cortex. J Neurosci 35:1089–1105.

Nguyen LH, Anderson AE (2018) mTOR-dependent alterations of Kv1.1 subunit expression in the neuronal subset-specific Pten knockout mouse model of cortical dysplasia with epilepsy. Sci Rep 8:3568.

O'Dell CM, Das A, Wallace Gt, Ray SK, Banik NL (2012) Understanding the basic mechanisms underlying seizures in mesial temporal lobe epilepsy and possible therapeutic targets: a review. J Neurosci Res 90:913–924.

Park SM, et al. (2018) Brain somatic mutations in MTOR disrupt neuronal ciliogenesis, leading to focal cortical dyslamination. Neuron 99:83–97.e7.

Pathak D, Guan D, Foehring RC (2016) Roles of specific Kv channel types in repolarization of the action potential in genetically identified subclasses of pyramidal neurons in mouse neocortex. J Neurophysiol 115:2317–2329.

Perez-Garci E, Bargas J, Galarraga E (2003) The role of Ca2+ channels in the repetitive firing of striatal projection neurons. Neuroreport 14:1253–1256.

Phelan KD, Mahler HR, Deere T, Cross CB, Good C, Garcia-Rill E (2005) Postnatal maturational properties of rat parafascicular thalamic neurons recorded in vitro. Thalamus Relat Syst 3:89–113.

Pineda JC, Galarraga E, Bargas J, Cristancho M, Aceves J (1992) Charybdotoxin and apamin sensitivity of the calcium-dependent repolarization and the afterhyperpolarization in neostriatal neurons. J Neurophysiol 68:287–294.

Powell CL, Brown AM (2021) A classic experiment revisited: membrane permeability changes during the action potential. Adv Physiol Educ 45:178–181.

Quiquempoix M, Fayad SL, Boutourlinsky K, Leresche N, Lambert RC, Bessaih T (2018) Layer 2/3 pyramidal neurons control the gain of cortical output. Cell Rep 24:2799–2807.e4.

Rathour RK, Malik R, Narayanan R (2016) Transient potassium channels augment degeneracy in hippocampal active dendritic spectral tuning. Sci Rep 6:24678.

Rizzo V, Richman J, Puthanveettil SV (2014) Dissecting mechanisms of brain aging by studying the intrinsic excitability of neurons. Front Aging Neurosci 6:337.

Rossini L, et al. (2021) Dendritic pathology, spine loss and synaptic reorganization in human cortex from epilepsy patients. Brain 144:251–265.

Shruti S, Clem RL, Barth AL (2008) A seizure-induced gain-of-function in BK channels is associated with elevated firing activity in neocortical pyramidal neurons. Neurobiol Dis 30:323–330.

Stedehouder J, et al. (2019) Local axonal morphology guides the topography of interneuron myelination in mouse and human neocortex. Elife 8:e48615.

Stiefel KM, Englitz B, Sejnowski TJ (2013) Origin of intrinsic irregular firing in cortical interneurons. Proc Natl Acad Sci U S A 110:7886–7891.

Strauss U, Kole MHP, Brauer AU, Pahnke J, Bajorat R, Rolfs A, Nitsch R, Deisz RA (2004) An impaired neocortical Ih is associated with enhanced excitability and absence epilepsy. Eur J Neurosci 19:3048–3058.

Subramanian L, Calcagnotto ME, Paredes MF (2019) Cortical malformations: lessons in human brain development. Front Cell Neurosci 13:576.

Swietek B, Gupta A, Proddutur A, Santhakumar V (2016) Immunostaining of biocytin-filled and processed sections for neurochemical markers. J Vis Exp 118:e54880.

Talos DM, Sun H, Kosaras B, Joseph A, Folkerth RD, Poduri A, Madsen JR, Black PM, Jensen FE (2012) Altered inhibition in tuberous sclerosis and type IIb cortical dysplasia. Ann Neurol 71:539–551.

Toledo-Rodriguez M, Blumenfeld B, Wu C, Luo J, Attali B, Goodman P, Markram H (2004) Correlation maps allow neuronal electrical properties to be predicted from single-cell gene expression profiles in rat neocortex. Cereb Cortex 14:1310–1327.

Tremblay R, Lee S, Rudy B (2016) GABAergic interneurons in the neocortex: from cellular properties to circuits. Neuron 91:260–352.

Varga C, Tamas G, Barzo P, Olah S, Somogyi P (2015) Molecular and electrophysiological characterization of GABAergic interneurons expressing the transcription factor COUP-TFII in the adult human temporal cortex. Cereb Cortex 25:4430–4449.

Williams SB, Hablitz JJ (2015) Differential modulation of repetitive firing and synchronous network activity in neocortical interneurons by inhibition of A-type K(+) channels and Ih. Front Cell Neurosci 9:89.

Wu ZZ, Li DP, Chen SR, Pan HL (2009) Aminopyridines potentiate synaptic and neuromuscular transmission by targeting the voltage-activated calcium channel beta subunit. J Biol Chem 284:36453–36461.

Wu S, Wei T, Fan W, Wang Y, Li C, Deng J (2021) Cell cycle during neuronal migration and neocortical lamination. Int J Dev Neurosci 81:209–219.

Wuarin JP, Kim YI, Cepeda C, Tasker JG, Walsh JP, Peacock WJ, Buchwald NA, Dudek FE (1990) Synaptic transmission in human neocortex removed for treatment of intractable epilepsy in children. Ann Neurol 28:503–511.

Wulff H, Zhorov BS (2008) K+ channel modulators for the treatment of neurological disorders and autoimmune diseases. Chem Rev 108:1744–1773.

Yang YM, Wang LY (2006) Amplitude and kinetics of action potential-evoked Ca2+ current and its efficacy in triggering transmitter release at the developing calyx of Held synapse. J Neurosci 26:5698–5708.

Zhao T, Wang L, Chen F (2024) Potassium channel-related epilepsy: pathogenesis and clinical features. Epilepsia Open 9:891–905.